



VEDURSTOFA  
ÍSLANDS

Report

R. Stefánsson, F. Bergerat, M. Bonafede, R. Böðvarsson,  
S. Crampin, K.L. Feigl, Á. Guðmundsson, P.G. Meredith,  
F. Roth, F. Sigmundsson, R. Slunga

## Earthquake-prediction research in a natural laboratory – PRENLAB-TWO

**Report**

**R. Stefánsson, F. Bergerat, M. Bonafede, R. Böðvarsson,  
S. Crampin, K.L. Feigl, Á. Guðmundsson, P.G. Meredith,  
F. Roth, F. Sigmundsson, R. Slunga**

**Earthquake-prediction research in a natural  
laboratory – PRENLAB-TWO**

**VÍ-G00008-JA03  
Reykjavík  
June 2000**

# Contents

<u>Summary</u> . . . . .	2
<u>Key words</u> . . . . .	2
<u>Introduction</u> . . . . .	2
<u>Methods and results</u> . . . . .	5
[1] Monitoring crustal processes for reducing seismic risk . . . . .	6
[2] Applying new methods using microearthquakes for monitoring crustal instability . . . . .	11
[3] Shear-wave splitting to monitor in situ stress changes before earthquakes and eruptions . . . . .	20
[4] Borehole monitoring of fluid–rock interaction . . . . .	23
[5] Active deformation determined from GPS and SAR . . . . .	27
[6] Effects of stress fields and crustal fluids on the development and sealing of seismogenic faults . . . . .	30
[7] Theoretical analysis of faulting and earthquake processes . . . . .	42
<u>References</u> . . . . .	62

# ENV4-CT97-0536

## EARTHQUAKE-PREDICTION RESEARCH IN A NATURAL LABORATORY PRENLAB-TWO

by

*R. Stefánsson, F. Bergerat, M. Bonafede, R. Böðvarsson, S. Crampin,  
K.L. Feigl, Á. Guðmundsson, P.G. Meredith, F. Roth, F. Sigmundsson, R. Slunga*

### Summary

The PRENLAB-2 project started in April 1998. It was a continuation of the PRENLAB project lasting from March 1, 1996, to February 28, 1998. It is a multidisciplinary multi-national scientific project to provide knowledge which can be a basis for reducing seismic risk. The questions which are raised are where, when and how will a destructive earthquake take place. The answers are sought by studying the relatively fast crustal processes at the plate boundaries in Iceland, on time scales ranging from geological time scales to current earthquake release. While the fast dynamic processes in the Iceland crust are one of the main pillars for the project another pillar is the high level seismic observation and evaluation seismic network, i.e. the SIL system.

### Key words

Mitigating risk, Hazard assessment, Multidisciplinary approach, Physical approach, Geodynamic approach, Modelling earthquake processes, Effects of crustal fluids, Stress direction changes, Microearthquake technology, Mapping of faults, Continuous GPS, SAR, Earthquake precursors, Premonitory changes, Stress forecasting, Short-term warnings, Database.

### Introduction

Among achievements of great significance for the project and for its outcome following can be mentioned:

- While Iceland as a whole is the test area for the project, the Hengill-Ölfus area has come to play a very significant role for the project (Figure 1). The reason is basically the very high seismic activity in this area since 1994. The seismic activity is a result of one hand the strain caused by transversal motion along the EW plate boundary in SW Iceland and on the other hand fluid expansion source near the center of the Hengill volcanic complex. It has been possible to carry out deformation measurements of various kinds to keep track of the deformation in addition to very detailed observations of frequent seismic swarms and individual earthquakes up to 5.1 in magnitude. Frequent observations by the SAR technology since 1993 show a steady uplift of 1.5 cm/year above a postulated pressure source at 7 km depth. The horizontal deformation is observed by GPS measurements, which have shown well constrained displacements related to individual earthquake sequences in two cases.

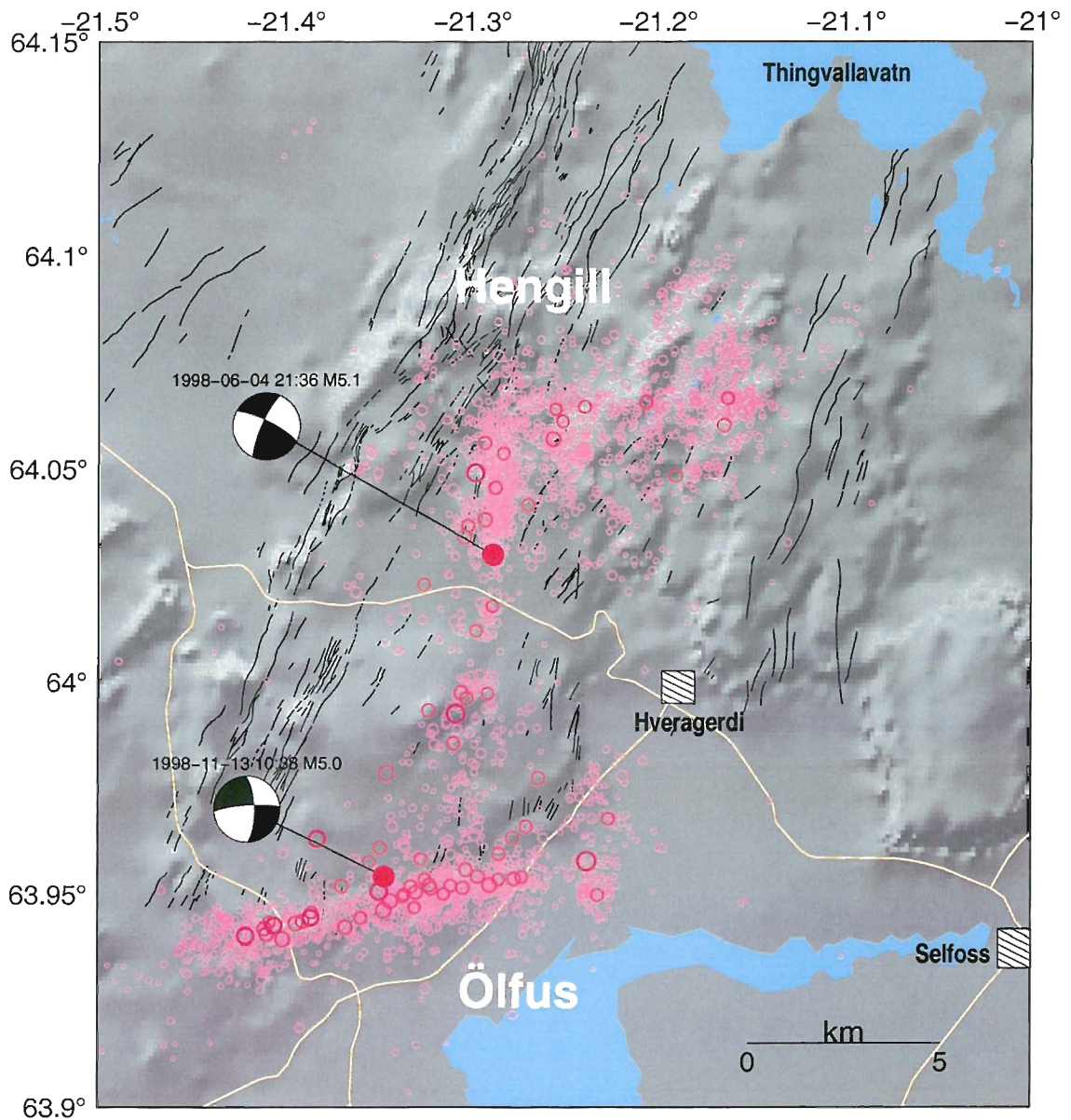


Figure 1. *The Hengill-Ölfus area is between the South Iceland seismic zone to the east, and the Reykjanes seismic zone and rift zone to the west. To NW goes the western volcanic zone. In this area there has been high seismic activity since 1994, which culminated in two earthquakes of magnitude 5 in 1998. These two earthquakes and related observed earth activity created research conditions which were of enormous significance for the progress of many parts of the PRENLAB-2 project.*

The stress modifications related to both of these earthquakes have been observed. Thus an earthquake cycle has been observed from the start time of build-up of stress on June 4, 1998, in a large area towards concentration of stress in a focal region and foreshocks of an earthquake that occurred on November 13, 1998. After the earthquake of November 13, it was then observed how an E-W fault zone served as a stress guide, and how a sequence of earthquakes was observed related to that guide. This has consequences for modelling large South Iceland seismic zone earthquakes which occur in sequences of earthquakes reaching magnitude 7.

- There has been significant progress in utilizing microearthquakes to study faulting processes. An automatic process has been developed to relate small earthquakes with individual fractures within an earthquake fault system on basis of very accurate relative location procedure and on basis of fault plane solutions. This opens the possibility to use microearthquakes to observe stable motion within a complicated fault system, changes of stresses and stress directions and earthquake nucleation. In seismology microearthquakes are mostly considered or treated as chaotic feature. By work in this field in the PRENLAB projects we are gradually discovering causality which in a physically understandable way relates the microearthquakes to each other and to larger events. Among significant indications of this mostly methodological study is that small earthquakes, also at depths near the base of the seismogenic crust, show similarity with hydraulic fracturing and changes in pore pressure that may have strong influence of the periodicity of and triggering of seismic activity.
- Very significant progress in observing relation between shear-wave splitting delay and deviatoric stress build-up has resulted in a successful stress forecast. On basis of experience in studying shear-wave splitting time patterns in the very active Hengill-Ölfus area in SW Iceland a successful stress forecast was issued. After a general information about increase in stress in the Hengill area in SW Iceland and on the basis of observations and modelling of nearby premonitory activity at end-October 1998, a definite stress forecast was issued by Stuart Crampin of the PRENLAB-2 project, on November 10, 1998. This forecast said that an earthquake of magnitude 5-6 could occur anytime between the issuing of the forecast ( $M=5$ ) and the end of February 1999 ( $M=6$ ) if stress kept increasing. An earthquake of magnitude 5 occurred near the center of the region included in the forecast on November 13. Although this kind of forecast is far from being a complete earthquake prediction this is a step forward for short-term warnings. It does not in itself specify the epicenter of the earthquake. In this case the most likely epicenter could be guessed based on former activity, i.e. to complete an ongoing seismic cycle. The earthquake itself had foreshock activity, which in fact defined the most likely epicenter for the earthquake, and also indicated that it was impending within short. Of course it is always a question if a sequence of small earthquakes is a foreshock activity or not. However, the pattern of foreshock activity in this case and methods for automatic evaluations of observations which are ongoing on basis of the collected data, give hopes that procedures can be developed to complete such a stress forecast by observations which aim at finding the place and the time of the earthquake nucleation before it ruptures.
- The current stress fields near the earthquake zones in North Iceland and in SW Iceland have been calculated by inverting a large number of fault plane solutions of the SIL system for stress. The average direction of extension was observed to

be N66°E for the Tjörnes fracture zone in North Iceland and N143°E for the area around the South Iceland seismic zone. This is in good agreement with the postulated pattern of the general divergent plate motion in Iceland. This result is also a significant base for studying the spatial and temporal variations in stress directions, which are related to uneven transversal plate motion and fluid intrusions, and thus to earthquake occurrence.

- Significant results have been obtained in geodetical and geological studies near the Húsavík-Flatey transform fault zone in northern Iceland. A model has been created mainly on basis of repeated GPS measurements which describes the fault system as a locked system down to a depth of 10 km but with a right-lateral transversal motion of 5 mm/year below that depth along the fault, i.e. the same sense of motion expected in a large earthquake on the Húsavík fault. Thus stress seems to be fast built up by time increasing the probability of a large earthquake in this area. Studies of aspect ratio of fluid filled veins studied in exposed parts of the Húsavík-Flatey fault zone indicate that fluid overpressure above the minimum compressive principal stress is 20MPa.
- Modelling work has been ongoing within some of the subprojects to explain observations of various kinds. A model has been developed to explain the historical earthquake sequence of the South Iceland seismic zone. This is a simple model assuming that the earth is a homogeneous halfspace and the plate divergency is constant, and that all the strain energy or stress build-up comes from the plate motion. The stress build-up in elastic lithosphere caused by magma upwelling from a medium with different rheological parameters has been modelled and studied with respect to earthrealistic conditions. A model has been proposed, based on modelling results and observations, which assumes that a significant part of the stress build-up before earthquakes comes from heat energy from the mantle. It is probable that basaltic fluids extracted from the Iceland mantle plume at depth of less than 100 km play a significant role, not only in triggering earthquakes in Iceland but also a significant role in the stress build-up. Work has started to develop such a model.
- Most significant extension of the observational network is that continuous monitoring of deformation has been initiated in Iceland by the installation of continuous GPS at 4 sites in an area of high seismic activity in SW Iceland, the Hengill-Ölfus area (Figure 2). These four stations are linked to observations of two former continuous GPS stations, which create a reference base for the local deformation monitoring. Observations and research within the PRENLAB-2 project of this activity, and the need to understand what is going on in this area, made it possible to obtain funds to start this innovating work. On the other hand the continuous GPS measurements provide new constraints in using the activity in this area as a basis for modelling earthquake processes.

## Methods and results

In the following the methods and results of the PRENLAB-2 project will be described in detail.

## 1 Monitoring crustal processes for reducing seismic risk

The work described here is basically a responsibility of IMOR.DG in cooperation with all the other groups involved in PRENLAB-2.

### Data collection

Much more work was carried out in data collection and data evaluation than anticipated when the workprogramme was prepared.

This was partly due to general extensions of the applied monitoring systems, but partly due to very high seismic and deformation activity in the Hengill-Ölfus area in SW Iceland (Figure 1). Enormously significant data were collected in this area which contain earthquake premonitory activity and short-term precursors to earthquakes, especially in June 1998 and in November 1998. The data collection and evaluations carried out in relation to this activity are of basic significance in understanding crustal processes leading to earthquakes, for modelling motions in an earthquake and for modelling the observed large-scale stress modifications that were caused by the two earthquakes [4].

The extension of the SIL seismological acquisition and evaluation system, the SIL system, has continued [16, 60]. The SIL system is a front line system with high level network facilities for detecting small signals and evaluating wave forms.

Quite often during high earthquake activity the incoming data of small earthquakes is so high in the SIL system that the communication system and the computers have problems to cope with the data stream, and jams were created, which sometimes could delay the data, so the system evaluation was delayed. This could even lead to loss of data. As it is very significant to gather earthquake data down to the smallest earthquakes, that provide information about crustal conditions, it was necessary to design and implement more effective procedures for doing this. For this purpose a new compression algorithm was developed for the system, i.e. the bit compression. This algorithm compresses the data very effectively at the site stations and the compressed data go directly into the evaluation procedures at the SIL center, much faster than the earlier procedures.

A new format for saving the digital earthquake waveform data will be described shortly in following:

The output of the seismometer digitizer is a series of integer values. The sample-to-sample variation is usually much less than the maximum values, which for most of SIL stations are between +/-3276800. In the AH format which was used by the SIL software, each value is stored in 32 bits.

A reduction in size of the data files of approximately a factor of 5 is achieved by storing the sample-to-sample variation in packed, variable size integers.

The access to data is thus much faster than to data that is compressed using general purpose compression programs such as gzip or compress and the files are typically 2-3 times smaller.

This new bit-compress format (bc) was incorporated into the data acquisition in the SIL system during the autumn of 1998. The software on each station writes in ascii files in format that is called the SIL format. The program bctool can convert these files to the bc format and back. All information in the headers is preserved.

The bc files are then transferred to the SIL center (currently using uucp). All files from each day are kept together, with a directory for each station. An index file that contains a list of all waveforms for each day is maintained.

The index files are stored on binary form, and are sorted by the programs that read

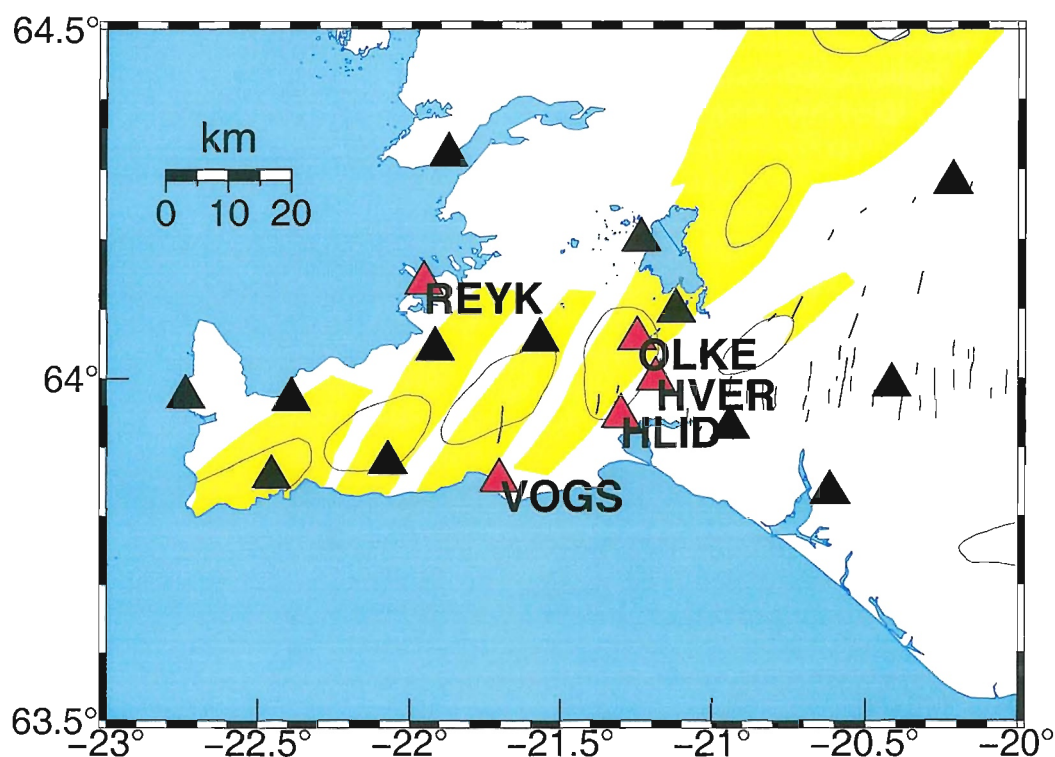


Figure 2. The figure shows the location of the new GPS network in SW Iceland, for continuous monitoring of deformations. Red triangles show the continuous GPS stations and the black triangles are the SIL seismic stations in the area.

them. A major performance bottleneck in previous version resulted from sorting index files on ascii form each time that waveform data arrived.

The new software is able to keep up with much larger levels of earthquake activity than previous software. Because the routines that read and uncompress the data are very fast and files are small, performance of all programs that use the data has been improved.

A build-up of continuous GPS monitoring at 4 sites in SW Iceland is a significant step forward for the PRENLAB-2 project data collection. It is significant for the watching the presently high seismic rate and deformation rate in the area. Four stations were installed in the Hengill-Ölfus area as shown in Figure 2.

The data processing is done at IMOR.DG, using the Bernese version 4.0 software from University of Berne. We are using data from the IGS station Reykjavík (REYK) as a reference station. The data from the network and results will be made available via the Internet. The URL is <http://www.vedur.is/ja/gps.html>.

A station for continuous monitoring of conductivity at depth in the crust by MT method was installed at the SIL station HAU, at the eastern end of the South Iceland seismic zone, and the data acquisition is merged with the SIL data acquisition. Changes of conductivity in the crust may provide significant information about conditions in the seismic zones.

### Data access

Work which started within the PRENLAB project of creating an earthquake database with easy access has continued and accelerated during PRENLAB-2. The database structure used is INGRES.

This database now contains SIL network seismic data since 1991 which can be accessed through the Internet, by search in a simple relational database table. This table has hypocenter and magnitude information on all SIL measured earthquakes since July 1991 that have been manually checked, approximately 140000 earthquakes. Search options for area, magnitude and time are provided.

The preparatory work for a general easy accessible relational database for all seismic data is completed and the inclusion of data in the database is in good progress.

Included in the database is already now or will be within short:

- Information based on historical information. This information has been gathered over the years and will be inserted into the database.
- Information on instrumentally measured earthquakes from 1926 to 1991. Available parameter data for earthquakes during the period 1926-1973 have been extracted from catalogues and is currently being inserted into relational database tables. Information on earthquakes that were felt but not recorded is also inserted into the tables.
- Information on SIL parameter data from 1991 to present. The data have been checked and updated to ensure compatible processing from different recording systems. The insertion of parameter data, both observed and derived, into relational database tables is nearly up-to-date. Information on approximately 140000 earthquakes is now accessible through a standardized SQL database.
- Information on station parameters, such as coordinates, instrument characteristics and time corrections at each respective time of measuring. Relational database tables have been developed.

Beside preparing this general database much work has been carried out in providing the various other subprojects with earthquake data, in accordance with the progress of the research work.

### **Enhancing the basis for alerts, warnings and hazard assessments**

This work has been carried out in relation to providing information and warnings about ongoing activity. It has been linked with increased probability of the occurrence of large earthquakes, on one hand in SW Iceland and on the other hand near the Húsavík earthquake fault in North Iceland.

Very much work which concerns all aspects of this task has been devoted to the Hengill-Ölfus area in SW Iceland. An earthquake sequence has been ongoing in this region since 1994, related on one hand to E-W transversal motion across the plate boundary, and on the other to an expansion source at 8-10 km depth below the Hengill area. The largest earthquakes of this sequence took place on June 4, 1998, magnitude 5.1, and on November 13, 1998, magnitude 5. The sequence of events, as observed seismologically and geodetically related to the time period of these events is of enormous significance for

understanding, build-up of stress before earthquakes and for understanding the nucleating process or the short-term precursor activity before earthquakes (Figure 3) [4, 52, 63].

After the earthquake of June 4, 1998, and the following earthquake sequence and deformation, stress was modified up to 50 km distance to east and west from the epicenter, along the E-W plate boundary. This appeared in widespread seismic activity, but also in increases in shear-wave splitting delay time, which lead to an earthquake forecast [22].

Work which is concerned with the possibility of an impending large earthquake, i.e. earthquake of magnitude 7, near the town Húsavík in North Iceland, was discussed at a special PRENLAB-2 workshop in Húsavík, July 30, 1998. Work is going on under several subprojects with risk related research in this region. This subproject has besides providing seismological data, taken initiative in planning new observations to be made in the area, on basis of the results of ongoing work. The objective is to provide observations which can create a better basis for modelling of the Húsavík earthquake, for an improved hazard assessment and for better real-time monitoring possibly involving short-term warnings [61].

Work is ongoing within this subproject regarding the Tjörnes fracture zone in general [52].

### **Modelling of near-field ground motions in catastrophic earthquakes in Iceland**

The  $M=5.1$  earthquake, June 4, 1998, in the Hengill area provided excellent geodetic and seismic data for modelling of near-field displacements in the largest earthquake in the area since 1955.

A large earthquake swarm started in the Hengill area on June 3, 1998, and culminated with a  $M=5.1$  earthquake on June 4, 1998, at 21:37 GMT, followed by thousands of aftershocks. Geodetic measurements were being done by the Icelandic Energy Authority at the time of the earthquake and repeated measurements begun on June 5, 1998. The data were processed by UICE.SI and NVI, using the IGS station in Reykjavík as a reference station, and CODE orbits. That provided the surface displacements in the ITRF96 reference frame.

The surface displacements have been used at IMOR.DG to construct a dislocation model for the earthquake. The dislocation model is a rectangular fault with uniform slip model in an elastic half-space. The best fit model found by nonlinear optimization algorithm, is a vertical N-S fault with 30 cm right-lateral strike slip motion and 15 cm dip-slip motion, down to west. The fault is about 11 km long, and extends from the surface down to about 2 km depth. The location of the fault model fits well with the location and focal mechanism of the main shock and locations of aftershocks, although these are not used to constrain the model. The model fits about 96% of the data signal (Figure 3).

The main shock ruptured a N-S structure, and could therefore be similar to historical events that have occurred in the South Iceland seismic zone, where a  $M=7$  event is currently anticipated. As there is no instrumental data for the large historical events it is important to study these recent earthquakes, to better understand the mechanism of the larger events.

Preparations are ongoing for modelling near-field ground motions expected in large South Iceland seismic zone earthquakes on basis of the result of the modelling above, on basis of strong motion records and records of the SIL network for the earthquake of June 4, described above, and on basis of historical documentation of near-field destruction in historical South Iceland seismic zone earthquakes.

## 2 Applying new methods using microearthquakes for monitoring crustal instability

### Investigation and monitoring of stable/unstable fault movements

#### Methods

The microearthquake analysis method which is used consists of inversion for fault plane solutions by use of spectral amplitudes and first motion directions [56, 50, 51] and multievent location based on high accuracy relative timing of the phase arrivals [58]. Both these algorithms are in routine use at the Icelandic seismological network within the PRENLAB-2 project. The multievent analysis aiming at inversion for the rock stress tensor is discussed in a later section.

The fault plane solutions do not consist of a unique fault plane solution for each event, but of a number of different fault plane solutions consistent with the observed spectral amplitudes and first motion directions. In addition each acceptable fault plane solution consists of two possible fault planes oriented such that the slip direction on one of the plane is normal to the other plane. Together this complicates the task to achieve a clear picture of what crustal deformation (fault movements) the microearthquakes are part of.

In a number of cases the relative locations of closely spaced similar microearthquakes have shown that such events often are situated on a plane which can be interpreted as the fault plane. This interpretation has also a sound physical basis as a slip on part of a fault will increase the instability at neighbouring areas if we have a rather similar rock stress tensor over the fault prior to the slip.

The most simple interpretation of a group of microearthquakes is to look for microearthquakes located along a plane and having acceptable fault plane solutions where one of its two possible fault planes coincides with the spatial plane. If one also requires that the slip directions on the plane are similar the process may be used to achieve a single fault slip solution for each microearthquake on the plane. The range of acceptable fault plane solutions has been reduced with no remaining ambiguity for the events of the consistent group.

In practice one will expect complications as the range of acceptable fault plane solutions may be large and random fits may occur. We will here give examples of multievent microearthquake analysis where this procedure for reducing the ambiguity of the fault plane solutions have been used.

#### The microearthquakes of the example

In Figure 4 a map of the epicenters and a depth section of the hypocenters of a group of events are shown. Also the map shows the double-couple source moment tensors of the fault plane solutions. The events have been located with the multievent location algorithm based on relative timing of the arrivals. The figure includes 470 events during November 13, 1998. The events are distributed with rms less than 800 m from a plane striking N77°E dipping 87°. This group of events are mainly aftershocks to a ML=5 earthquake. The ML values are in the range 0.5-2.0 for most of the events.

Note that the horizontal stress directions are very consistent and dominated by SW-NE compression. If we look on the source moment tensors along the direction of compression it can be seen that the events have a small normal faulting component in addition to the generally dominating strike-slip component.

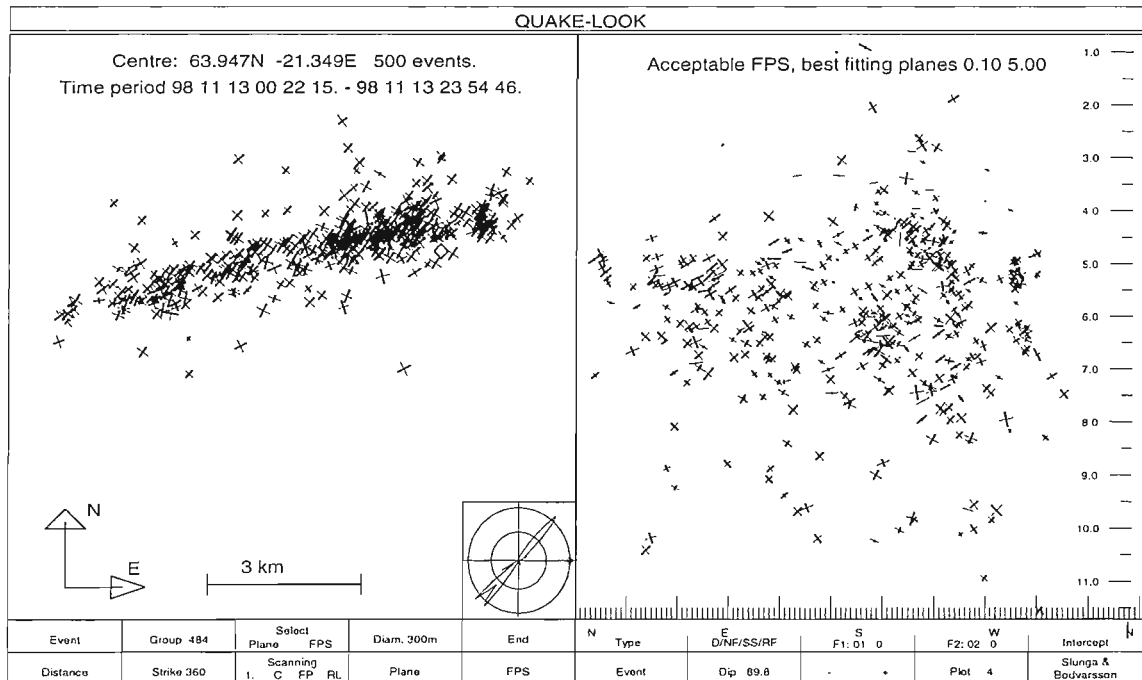


Figure 4. This figure illustrates the double-couple source moment tensors of the fault plane solutions. The representation is the same as in [57], and the thick line shows the subsidiary compression and the thin line shows the subsidiary extension. The distribution of the horizontal compressions (the thick lines of the left map) are shown in the small circle. The right part shows the unscaled frequency (number of events), the left part is scaled according to seismic moment.

### Automatic relating of the earthquakes to individual fractures

An automatic procedure of grouping the events was applied based on their locations (a plane) and the consistency of their acceptable fault plane solutions (plane orientation similar to the spatial plane and similar slip directions).

Of the 470 events within the group the automatic algorithm included 115 events within 15 groups. For each of these 115 events we thus have a proposed unique fault plane.

These groups define a complicated set of fractures with defined strikes and dips. These are identified with known fracture and rift zone directions on the surface.

### Discussion of picture of the seismic activity given by the automatic grouping

The sizes of the fractures have typically dimensions of several kilometers both laterally and vertically. The number of events on the same fracture is mostly only 6-9 and the estimated fault radii are mostly less than 200 m. As an example in Figure 5 we see a view of the earthquakes within the dominating W-E group. The events are fairly well spread over the fracture. The sizes are the real sizes as given by the corner frequency estimates [50]. Even if the total number of events during this day is 5 times more the surfaces of the events will not cover the whole fracture area. The time order of the events over the area is rather random, not like a domino game. Figure 6 shows the same events as Figure 5 but now scaled according to slip size (the area of the event circles are proportional to slip size). The conclusion is that the size of the seismic slip during this day is very unevenly distributed over this fracture and that the activity starts at several places not neighbouring to each other.

### *Similarity to hydraulic fracturing*

If the pore pressure is increased in a rock mass the pore pressure will first increase along certain fractures with highest permeability. If there remains shear stress over this fracture the pore pressure increase will trigger seismic events at locked asperities. The pore pressure will also increase in fractures crossing the main fracture and trigger slip on those fractures. This activity is initially expected to occur close to the first fracture and later spread out.

The pattern we see here with a seismic activity spread along a main fracture and with activity on crossing fractures is very similar to what can be observed during hydraulic fracturing of rock masses through water injection. Thus it is possible that increase in pore pressure is affecting the period of seismic activity.

### *Stable and unstable fault slip*

The seismicity is the unstable slip on the fracture. Stable brittle slip is not seismically observed but is a possible cause to seismic activity at different places over a fault area within a short-time window. The reason is simple that if a fault starts to slip stably as a whole it is likely that some asperities will remain locked, accumulate stress concentration due to surrounding fault slip, and then break seismically when the stress is too large. The size of the slip depends then on the strength of the locked part. In Figure 6 showing the peak slips of the events on the possibly primary fault there are three events having significantly larger slip. The peak slips of those events are 3-7 mm. The first events on this fracture have all small peak slips, less than 1 mm. Then the deep 3 mm event appears while smaller slip events continue to occur at "normal" (4-7 km) depth. After 7 hours the upper 3 mm event occurs and after 10 hours the 7 mm event comes. This picture is in reasonable agreement with what one might expect if the fracture started to slip stably

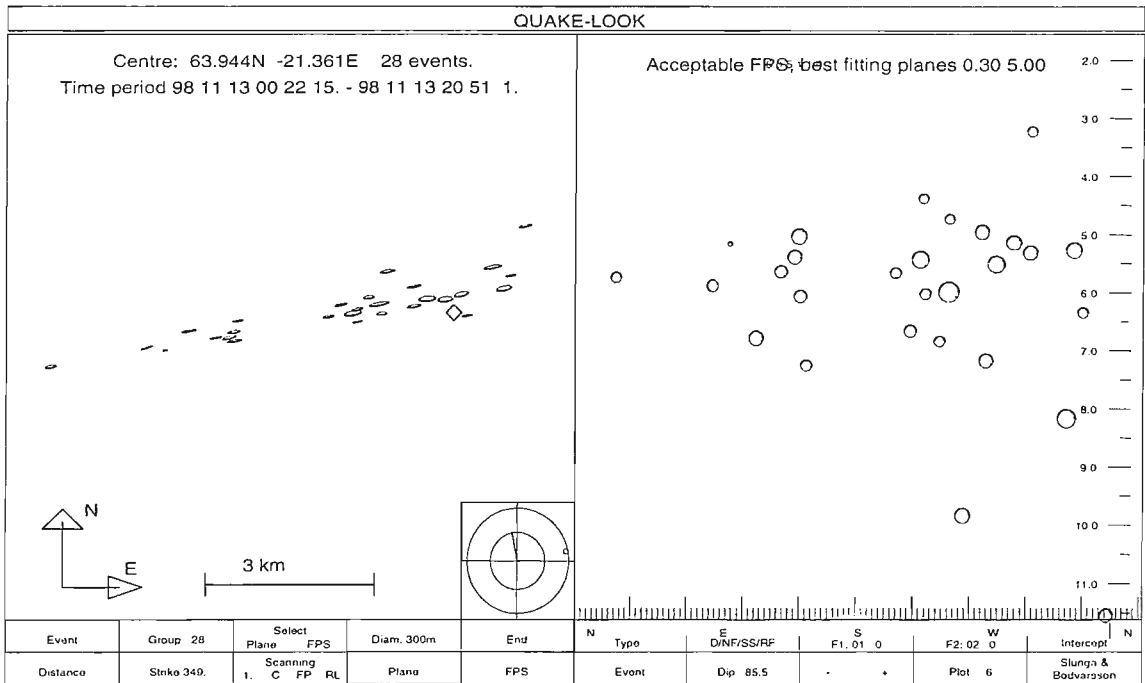


Figure 5. This figure shows the 28 events of the largest group striking  $N79^{\circ}E$ . The view to the right is normal to this strike ( $N21^{\circ}W$ ). The sizes are now not scaled but the true ones as estimated from the corner frequencies. The slip directions (marks at the peripheries) are not perfectly consistent but the slips are mainly in the same direction. Note that the fracture surface is not covered by these events which may indicate stable slip between the events.

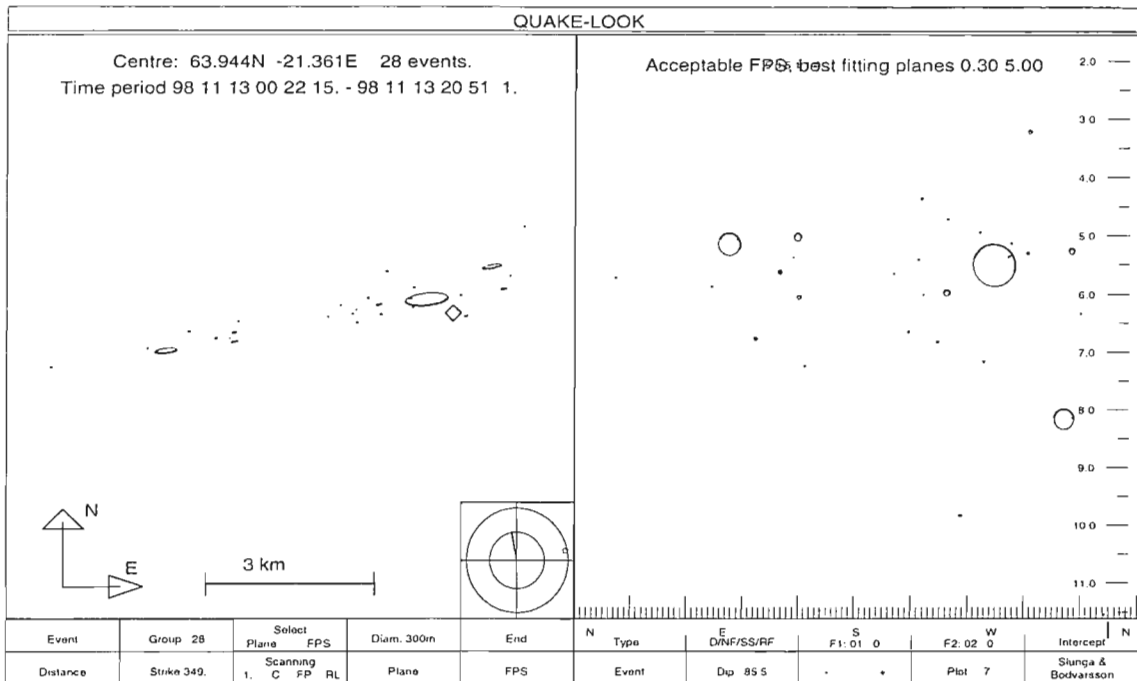


Figure 6. As Figure 5 but now the events have been scaled according to slip size. The largest slip is 7 mm, the next largest are around 3 mm. The diameters of the event "coins" are proportional to the slip size. Note that the three largest events (slips) have very consistent slip directions. If the slip on this fault has been constant over the whole area most of the slip must have been stable (non-seismic).

at the time of the main event. Possibly the deeper part has started to slip earlier or at a higher rate.

It is of course not the purpose of this simple example to reach any conclusion, the reason of presenting this discussion is to indicate what eventually will come out if more extensive and intensive analysis of this type continues in the area.

The assumption of a general stable slip process triggering seismic events at asperities indicates that the stable slip over this single fracture during the day is at least 7 mm which is the largest slip of a single event on the fracture. One must, however, remember that it may be possible that the 7 mm event was already prestressed and was triggered by a smaller stable slip. This is, however, something that can be analyzed, a 7 mm movement on a large fault area will affect the stability in its close surroundings and can be expected to be consistent with occurrences and mechanisms of the surrounding microearthquake.

#### *The time development of the slip sizes on the different fractures*

Only six of the 15 fracture groups contain events having peak slips exceeding 1.5 mm. Of these 4 shows a rather strict decay of the slip sizes with the largest slips within 2 hours of the main shock. One group has a rather irregular time development with the largest slip event about 5 hours after the main shock. This is one of the N-S striking fractures. Only the largest group, 28 events on the W-E fracture, shows a rather clear increase in the slip sizes with time and with the largest slip event at the end of the day and at the east end of the fault (east of the main event which is on a N-S fracture on the north side of the W-E fracture).

The N-S group having an unclear slip development with time is far from vertical and

is at the east end of the activity. It may be that this activity is affected by the possibly increasing slip on the W-E fracture where the slip increases with time.

The activity prior to this day migrated from west along a western extension of the activity of Figure 4. Together with the indications that the W-E fault started to slip at the time of the main event, it seems possible that the main event was associated with some locking of the W-E fracture of the 28 events.

### Conclusions

There are several indications that the automatic grouping of the events applied after multievent location (based on relative timing) and after singleevent fault plane solutions (based on spectral amplitudes and first motion directions) results in groups of events associated with fractures that may be real. It is not possible to come to definite conclusions from only one investigation of this type. The PRENLAB projects produce, however, much more data, this example was based on only one day of activity. As not only the grouping algorithm is automatic, but also the fault plane solution algorithm and the multievent algorithm there are no real problems to submit all data to such a detailed analysis as given here. This little study is part of the preliminary work of how to implement this multievent analysis to all data. The point is not whether the tentative possible results of this example are true or not. The point is that studies like this do not demand a lot of work. When all data are interpreted in this way it is likely that altogether the significance will increase so there will be obvious results and not only indications.

Although there seems to be no chaos among the small earthquakes (for instance the very high horizontal stress consistency) the picture seems to be complicated as so many small fractures are involved. However, with use of computers the complexity is no real problem as it easily can be handled.

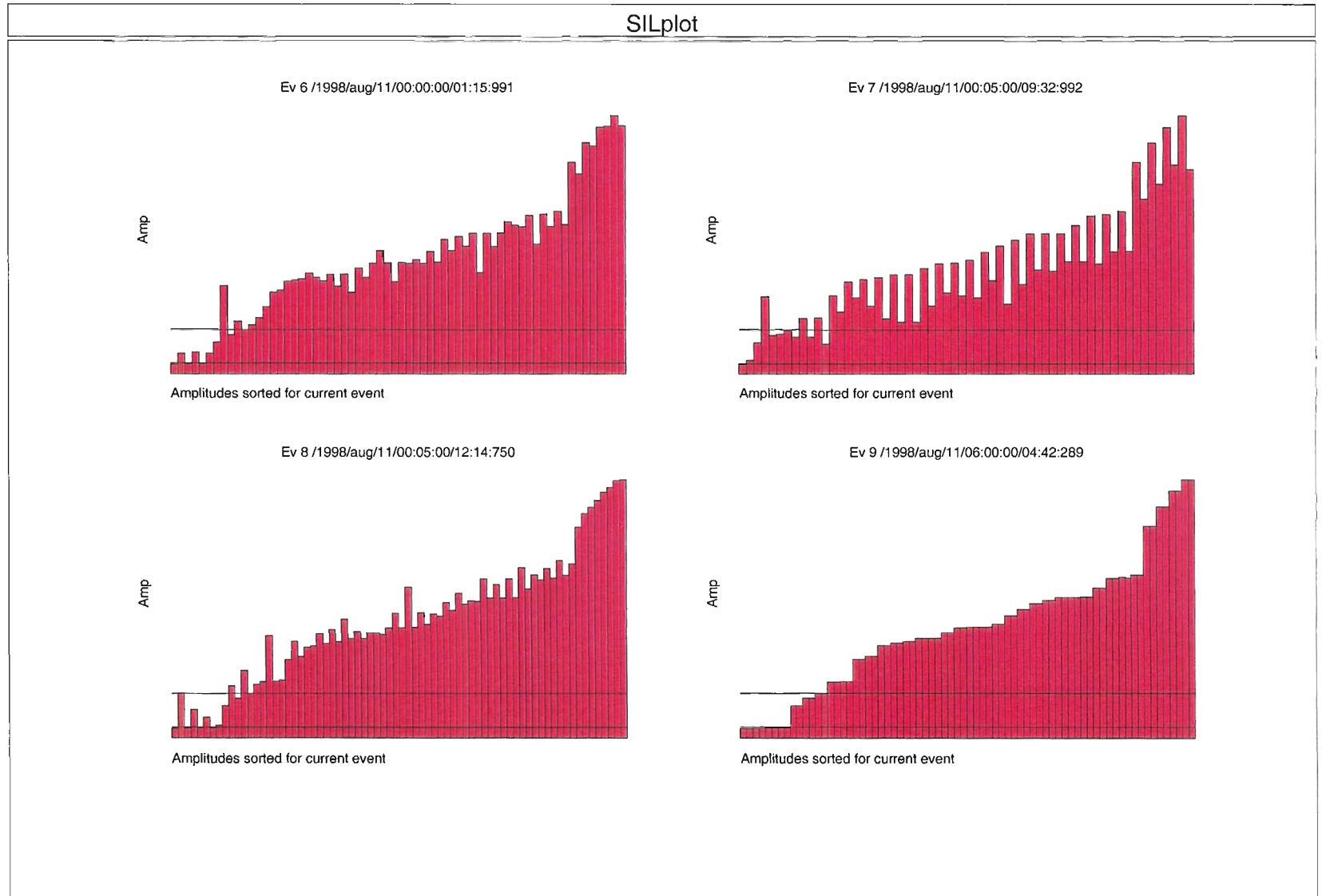
The coming work will partly go to develop the type of studies here to routine algorithms for analyzing all data, and partly to analyze the physical interaction of the different fracture slips. The hope is that the physical interaction will be of great help in reducing the uncertainty of the tentative interpretations.

### **Spectral amplitude correlation**

Rather than only working with hypocenters of single earthquakes we chose to relate the statistical analysis with stress tensors derived from number of microearthquakes limited in time and space. Before applying the stress tensor inversion we pre-process the dataset to minimize the time/space span but ensuring stable stress tensor solution. For this we have developed a algorithm based on correlation of spectral amplitudes. The SIL network frequently records swarms of microearthquakes where the individual events in the swarm occur very close to each other and often the events can be interpreted as occurring on the same fault. Assuming that this interpretation is correct and that the events in the swarm have similar slip directions, the radiation patterns from these events will be very similar. We should thus be able to observe strongly correlated amplitude and polarity recordings from the events in such a swarm.

We investigated amplitude recordings from a swarm of microearthquakes in Ölfus in SW Iceland. Since the events were not always registered by the same number of stations, or had the same number of phases registered at the stations, we picked out stations and phases common to the two events we wanted to compare. Shown in Figure 7 is a comparison of four events. Each of the pillars in this figure are spectral amplitudes (DC-level) of P-radial – P-vertical, SV and SH at 9 stations. Event number nine, in the lower

Figure 7.



right corner, is compared to itself and to events six to eight. For each event pair we sorted the logarithm of common phases according to ascending order of event nine's amplitudes and then plotted the two events common amplitudes next to each other. Since event nine is compared to itself in the lower right the amplitude pairs are exactly the same height. For the other three plots we see that the amplitude pairs are not identical but that there is great similarity in the shapes of the amplitudes.

A cross-correlation algorithm was constructed which calculates the linear correlation coefficient for all pairs of events in a dataset. Only common amplitudes above the threshold are included in each correlation, and the logarithms of the amplitudes are used in order to down weight the importance of the amplitudes at the closest station, which would otherwise dominate the correlation.

#### Composite focal mechanisms

The groups obtained by the amplitude correlation contain closely located events with very similar radiation patterns. This suggests that we could calculate a well constrained, composite focal mechanism for the events by stacking amplitude and polarity observations. The focal mechanism thus obtained would give more accurate information about the nodal plane orientations and slip directions, however, the dynamical parameters would be a mere average of the events in the group. We implemented an algorithm that normalizes the amplitudes of the individual earthquakes to the median amplitude for the event. These normalized amplitudes are then stacked, for each phase on all available stations, and the final result is renormalized with the median of the event medians. Polarities are stacked at each station and the median polarity used as the correct one at the station. In our test group the composite mechanism was calculated from amplitudes at 11 stations and using seven polarities, to be compared to the individual events median of eight stations and two polarities. This work is still in progress but preliminary results show that the optimal fault plane solution obtained from the composite event show very good agreement with the estimate of the fault plane orientation from relative location.

#### Preprocessing stress tensor inversion data

One of the purposes of the amplitude correlation method was to investigate the possibility of reducing the number of similar events in our stress tensor inversion scheme [46]. Events having very similar focal mechanisms do not contribute any independent information to the stress tensor inversion and since the inversion is rather slow we would like to reduce the number of events in each inversion as much as possible without affecting the result. Amplitude correlation is one possible way of performing such a reduction. Figure 8 shows the inversion results using all 100 events in the Ölfus dataset in the upper section of the figure. Below is the result obtained after removing 54 events considered similar by the amplitude correlation algorithm. There were 6 groups of similar events, with a total of 60 events in the groups. We retained the event with the largest number of stations and phases as the representative for each group. We see that there are more normal faulting stress states after the reduction but that the overall stress state is rather similar to the inversion with all events. We aim toward a better match between the stress results obtained after reduction with the original and we are in the process of investigating the use of composite fault plane solutions as representatives of the groups and a more accurate calculation of the confidence limits.

# Ölfus

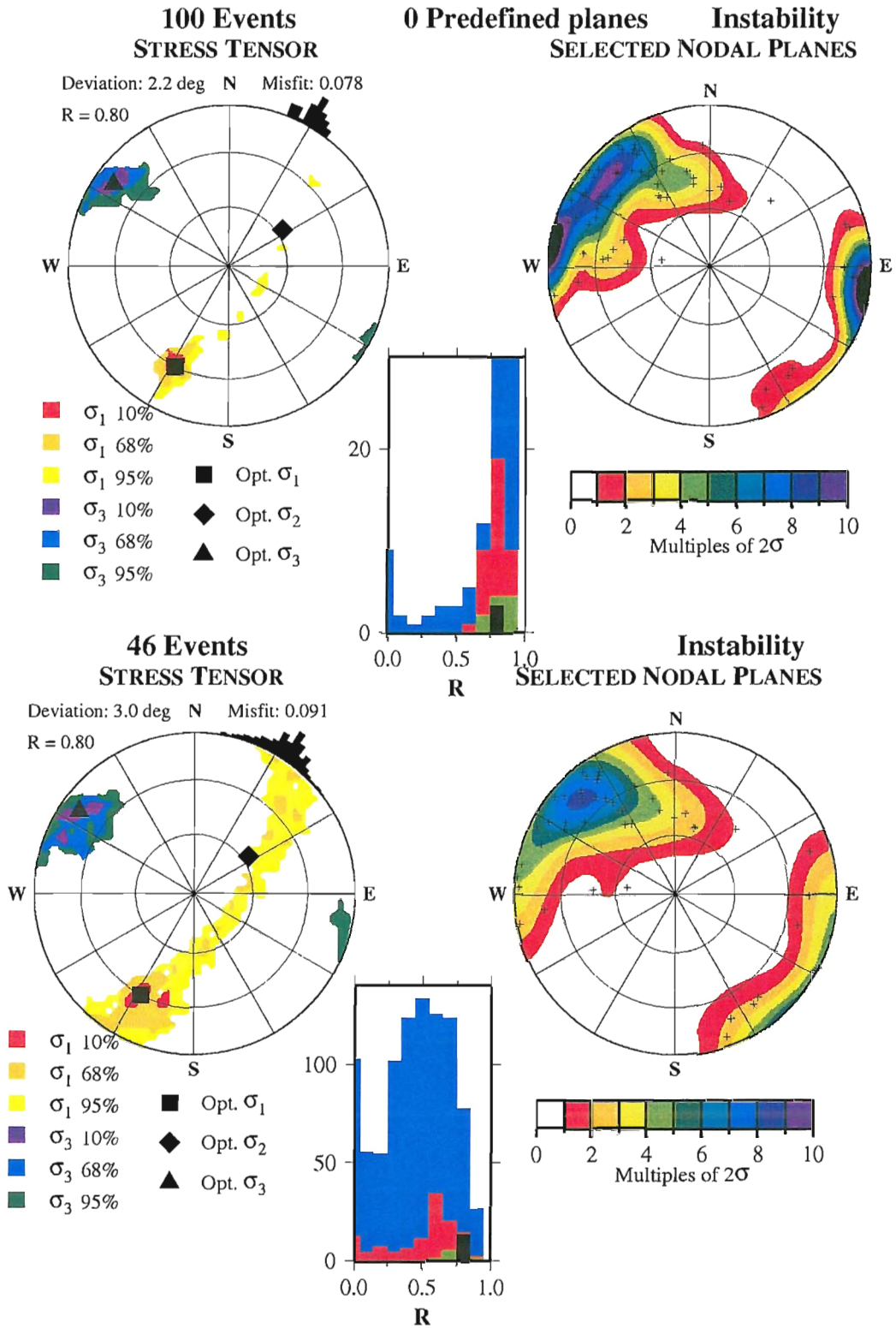


Figure 8.

### 3 Shear-wave splitting to monitor in situ stress changes before earthquakes and eruptions

Shear-wave splitting (seismic bi-refringence) is widely observed in all crustal rocks worldwide, whenever there are small earthquakes within the shear-wave window of seismic stations [18, 19]. Caused by stress-aligned fluid-saturated grain-boundary cracks and pores, the microcracks are highly compliant to changes in stress, and changes in shear-wave splitting have been seen before four earthquakes worldwide [18, 19]. These changes are now seen routinely before earthquakes in the transform zone of the mid-Atlantic ridge in SW Iceland [22].

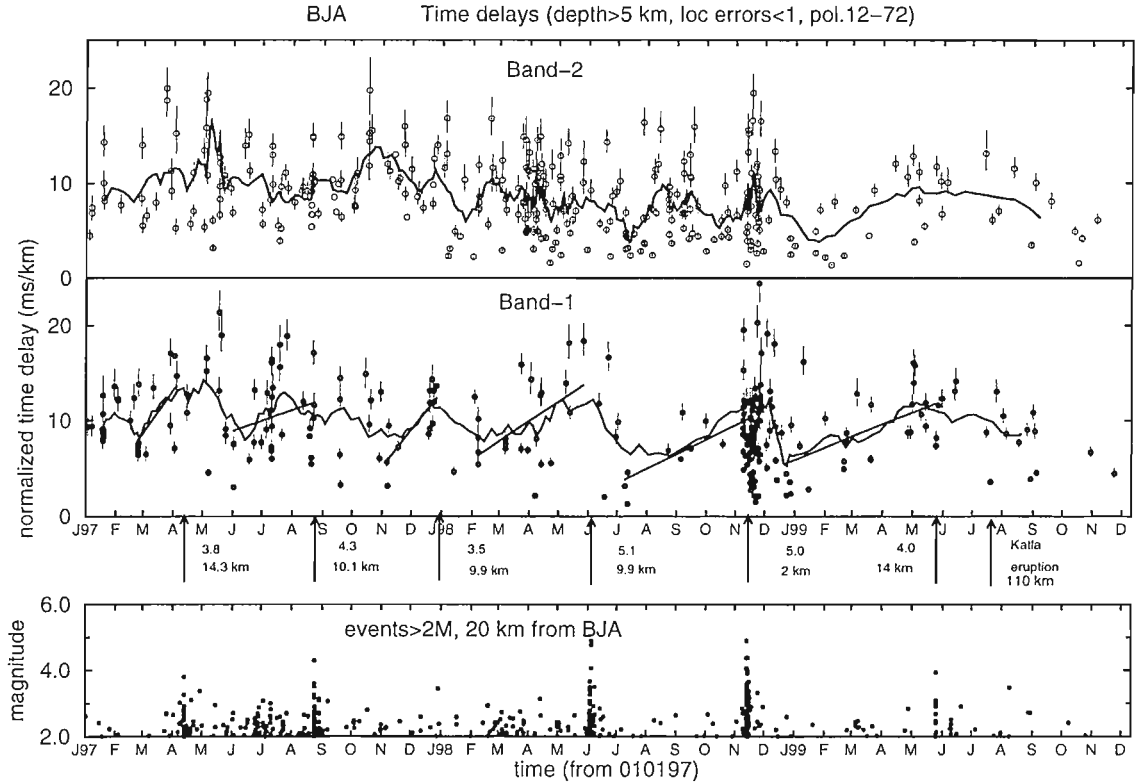


Figure 9. Time-delays between split shear-waves in Band-1 (middle cartoons) and Band-2 (upper cartoons) of the shear-wave window at station BJA for earthquakes below 5 km-depth from January 1, 1997, to December 1, 1999, normalized to ms/km, and plotted against time. There are nine-point moving averages through the time-delays in both bands. Middle cartoons (Band-1) show least squares straight-lines beginning near minima of the nine-point average and ending at a larger earthquake. Only reliable time-delays (errors less than 0.5 ms/km) are plotted and error bars are derived from location errors less than 1 km. Lower cartoons are earthquakes ( $M \geq 2$ ) within 20 km of the recording stations.

Figures 9 and 10 shows changes in shear-wave splitting from January 1, 1997, to December 1, 1999, at stations BJA and KRI in SW Iceland. The time-delays between the split shear-waves, normalized to ms/km, are shown in two bands. The middle diagrams show time-delays in Band-1 [22], which are sensitive to changes in crack aspect-ratios and it has been demonstrated [19] that the immediate effect of increasing stress is to modify crack aspect-ratios. The upper diagrams show time-delays in Band-2 which are sensitive

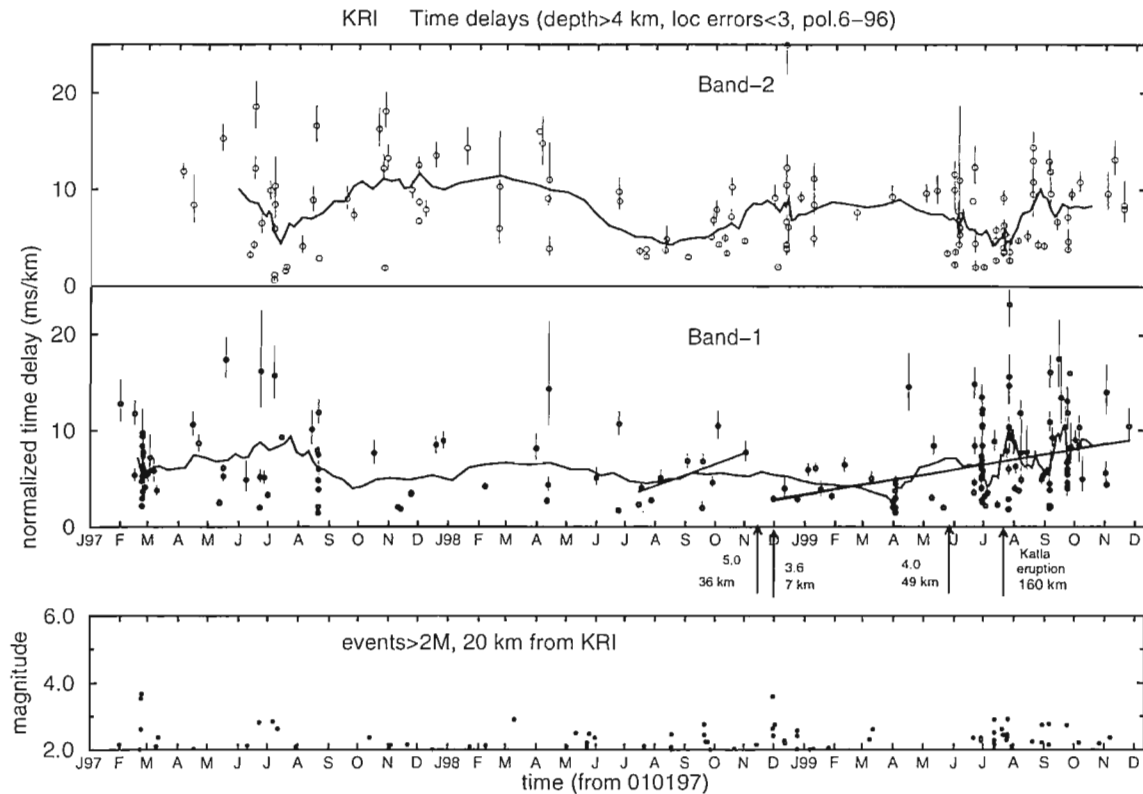


Figure 10.

to crack density. The lower diagrams show the magnitudes of earthquakes within 20 km of the stations.

Both bands of time-delays have nine-point moving averages. The time-delays in Band-2 show no identifiable correlation with the earthquakes. The time-delays in Band-1 have least-squares lines added to data where the averages show increases. These least-squares lines begin just before minima of the moving average and end where there is a larger earthquake nearby marked below the diagram. The first four increases at station BJA show regular behaviour. It was recognized towards the end of October 1998 that another increase had begun. This allowed the successful stress-forecast of the time and magnitude of a  $M=5$  earthquake on November 13, 1998 [21, 22] (see the exchange of emails between UEDIN.DGG and IMOR.DG listed in Table 1).

Note that changes in shear-wave splitting do not provide information about the location of the forecast event, but IMOR.DG recognized continuing seismicity from a previous event and suggested correctly that the forecast event would occur on a fault close to station BJA [22].

Note changes in Band-1 monitor the effect of changes of stress in microcrack geometry. Stress changes before volcanic events also effect shear-wave splitting. The overall decline in time-delays in both bands at both stations follows increases first identified before the Vatnajökull eruption, and is believed to represent the adjustment of the mid-Atlantic ridge to the effect of the eruption.

In 1999, changes in shear-wave splitting at BJA do not show the previous regular behaviour. This is believed to be due to volcanic activity at the volcano Katla which erupted in July 1999.

Time delays in Band-1 at station KRI show an exceptionally large scatter but there

October 27	UEDIN.DGG emails IMOR.DG reporting shear-wave time-delays in Band-1 increasing from July at stations BJA and KRI and suggests: ". . . <i>there was an 80% chance of something significant happening somewhere between BJA and KRI within three months.</i> "*
October 28	UEDIN.DGG faxes data for BJA and KRI to IMOR.DG. IMOR.DG suggests M=5.1 earthquake near BJA in June 1998 may be linked to current increase in time-delays.
October 29	UEDIN.DGG updates current interpretation and suggests: " <i>Shear-wave splitting at both BJA and KRI indicate something is going to happen soon, probably within a month . . .</i> "*
October 30	IMOR.DG sends notice to National Civil Defence (NCD) in Reykjavík suggesting a meeting.
October 31 -November 4	Faxes and emails updating information. UEDIN.DGG refines data and interpretation. IMOR.DG creates local geophysical and geological investigations.
November 5	IMOR.DG presents stress-forecast and other data from surrounding area to scientific advisors of NCD, who conclude no further action was required of them.
November 6-9	Exchange of various faxes and emails updating information and interpretation.
November 10	UEDIN.DGG concludes: ". . . <i>the last plot . . . is already very close to 10 ms/km. This means that an event could occur any time between now (M≥5) and end of February (M≥6) .</i> "*
November 11	UEDIN.DGG faxes updated data for KRI and BJA, with SAU now also suggesting increasing time-delays from September.
November 13	IMOR.DG reports: ". . . <i>here was a magnitude 5 earthquake just near to BJA (preliminary epicenter 2 km west of BJA) this morning at 10:38 GMT.</i> "*

Table 1. *Timetable 1998, e-mails, facsimiles, and actions. \*Quotations ("italics") are exact texts from e-mails.*

is consistent increase since December 1998. At one year, this is the longest duration of increase yet observed in Iceland. Assuming that the impending event is close to station KRI, and assuming linearity, the increase will reach the level of fracture-criticality (11 to 14 ms/km at BJA) between February and July 2000. Note, however, that linearity cannot be assumed, neither can it be assumed that the increase is due to an impending earthquake, and the size of a volcanic event is probably not directly related to the duration or rate of increasing time-delays. All we can suggest is that a big event (M≥6 earthquake or volcanic eruption) is approaching. Since no clear evidence of an increase can be seen at BJA or SAU this suggests that the event will be probably be at the west end of the Reykjanes peninsula.

Note: Stress-forecasts using small earthquakes as a source of shear-waves can only made in areas of exceptionally persistent small earthquakes. To stress-forecast earthquakes elsewhere would require the development of stress-monitoring sites (SMSs) where shear-wave splitting is monitored in cross-well seismics. This was first suggested in 1998 [17]. The recent commercialization of an effective shear-wave source now allows much cheaper borehole geometries [21], and the EC has recently funded the development

of a SMS near Húsavík on the Flatey-Húsavík fault in northern Iceland [23].

#### 4 Borehole monitoring of fluid–rock interaction

In the framework of the PRENLAB projects, repeated loggings are carried out to obtain a time series of logs in the South Iceland seismic zone (SISZ)(Figure 11). An 1100 m deep borehole (LL-03, “Nefsholt”) inside the zone (63.92°N, 20.41°W, 7 km south of the seismic station SAU) is used and provides the unique opportunity to perform measurements much nearer to earthquake sources than usual – the hypocenter depths at that location range between 6 and 9 km. Moreover, data can be obtained for a depth interval of more than 1000 m, uninfluenced by the sedimentary cover and less disturbed by surface noise.

In the preparatory phase of an earthquake, stress accumulation is expected to be connected with the creation of borehole breakouts (BOs), changes in the number and size of cracks, a possible variation of the stress direction, etc. Therefore, the following set of geoparameters is monitored:

- P-wave travel time.
- Electrical conductivity.
- Stress information from borehole breakouts (orientation and size).
- Crack density.

This is achieved by repeated logging with tools as:

- Sonic log (BCS).
- Gamma-ray (GR).
- Spectral gamma-ray (SGR).
- Dual induction/latero log (DIL).
- Neutron–neutron log.
- 16"- and 64"-resistivity log.
- Spontaneous potential log (SP).
- Four–arm–dipmeter (FED).
- Borehole televiewer (BHTV).

The neutron–neutron log, the 16"- and 64"-resistivity log and the SP log are run with the logging equipment of Icelandic Energy Authority, the rest with the Halliburton logging truck of GFZ.DR.DBL.

##### *Investigations on the stress field in the SISZ:*

Besides the repetition of logs in borehole LL-03 Nefsholt, we performed single logging campaigns at other boreholes to check the state of the regional stress field. This is important for two reasons:

- From the San Andreas fault we know that fault zones may be in a low stress state between earthquakes, which gets visible through stress orientations perpendicular to the strike–slip fault instead of pointing at it under an angle of 30° to 45°. To determine the present state of stress in the SISZ, it is important to see if there are stress components, that are not perpendicular to existing faults and favour earthquakes on them.
- The SISZ is no typical transform zone. Looking at the orientation of opening at the adjacent rifts, one would expect a left–lateral strike–slip zone in roughly E-W

direction (N103°E) to connect the Reykjanes ridge and the eastern volcanic zone of Iceland. Instead earthquakes occur on en-echelon N-S striking right-lateral faults. Assuming an angle of 45° between the maximum horizontal compressive stress and the fault (as it is done constructing fault plane solutions) both planes are equivalent. From a rock mechanics point of view, expecting an angle of about 30° between fault and maximum horizontal principal stress, the stress orientation at N-S striking faults should be N30°E, compared to N60°E at an E-W striking transform.

Well:	Logged interval:	Interval with BOs/vertical fractures:	Total length of BOs/vertical fractures:	Orientation of $\sigma_H$ :	Standard deviation:
BS-11	703-1090 m	713-934 m	45.0 m fract.	N45°E-N90°E	—
LL-03	80-1100 m	780-983 m	5.0 m BOs	N30°E	12°
THB-13	466-1225 m	925-941 m	3.5 m BOs	N21°E	10°

Table 2. *Stress orientations found at SISZ from borehole televiewer logs.*

#### *Results:*

The results can be summarized as follows:

- The repeated measurements of sonic P-wave velocity and the latero log resistivity show good repeatability.
- The repeated resistivity measurements with the dual induction log (deep and medium penetration) show a change between the logging campaigns in September and December 1997. The values of voltage of the induction log with deep penetration generally increased and the values of the induction log with medium penetration generally decreased. No correlation to any seismic activity or other observations was found, so far. Investigations on possible reasons are still going on.
- The stress orientations found at all three locations are similar and agree with a left-lateral strike-slip regime. They are not perpendicular to existing ruptures found for large earthquakes in the SISZ and therefore indicate that the SISZ is not a weak fault, as postulated for the San Andreas fault. Borehole breakouts observed in Nefsholt and Þykkvibær show the maximum horizontal principal stress at an azimuth of approximately NNE (N21°E to N36°E) (Figure 12 and Table 2). The data obtained in Böðmódsstaðir show an average direction of maximum principal horizontal stress ENE (Figure 13 and Table 2). Thus, the direction of maximum principal horizontal stress, as found by the borehole televiewer data, varies from NNE (north of the SISZ, BS-11) to ENE (south of the SISZ, THB-13). This NNE variation is slightly more than the standard deviation. From a rock mechanics view, the stress directions found at Nefsholt (LL-03) and Þykkvibær (THB-13) fit to N-S striking faults, as they are found in the SISZ. On the other hand, the orientation of maximum horizontal principal stress found at Böðmódsstaðir fits to the model of an E-W striking transform fault zone. Similar stress orientations have also been found from fault plane solutions [60]. This was confirmed when a mean orientation of  $\sigma_H$  of N56°E derived from 1916 fault plane solutions quality selected from 4413 earthquakes in the SISZ during the years 1995 to 1997 was found [3]. A NE-SW orientation of  $\sigma_H$  was also the result of investigations on shear-wave splitting due to crustal stress anisotropy at four of six seismic stations in the SISZ [62].

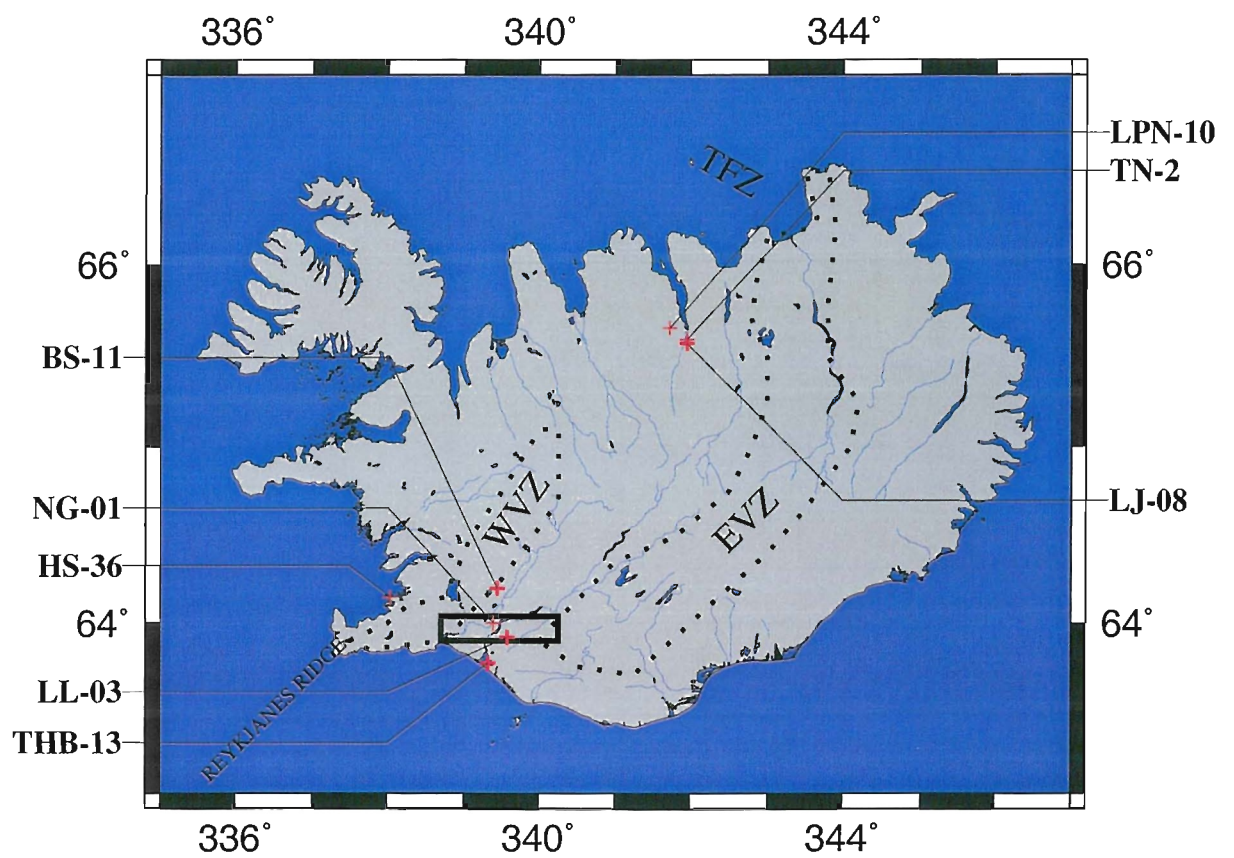


Figure 11. Map of Iceland showing the location of the site of repeated logging (Nefsholt) and of the other boreholes, where measurements have been performed. The box in SW Iceland indicates the orientation and the length of the South Iceland seismic zone (SISZ).

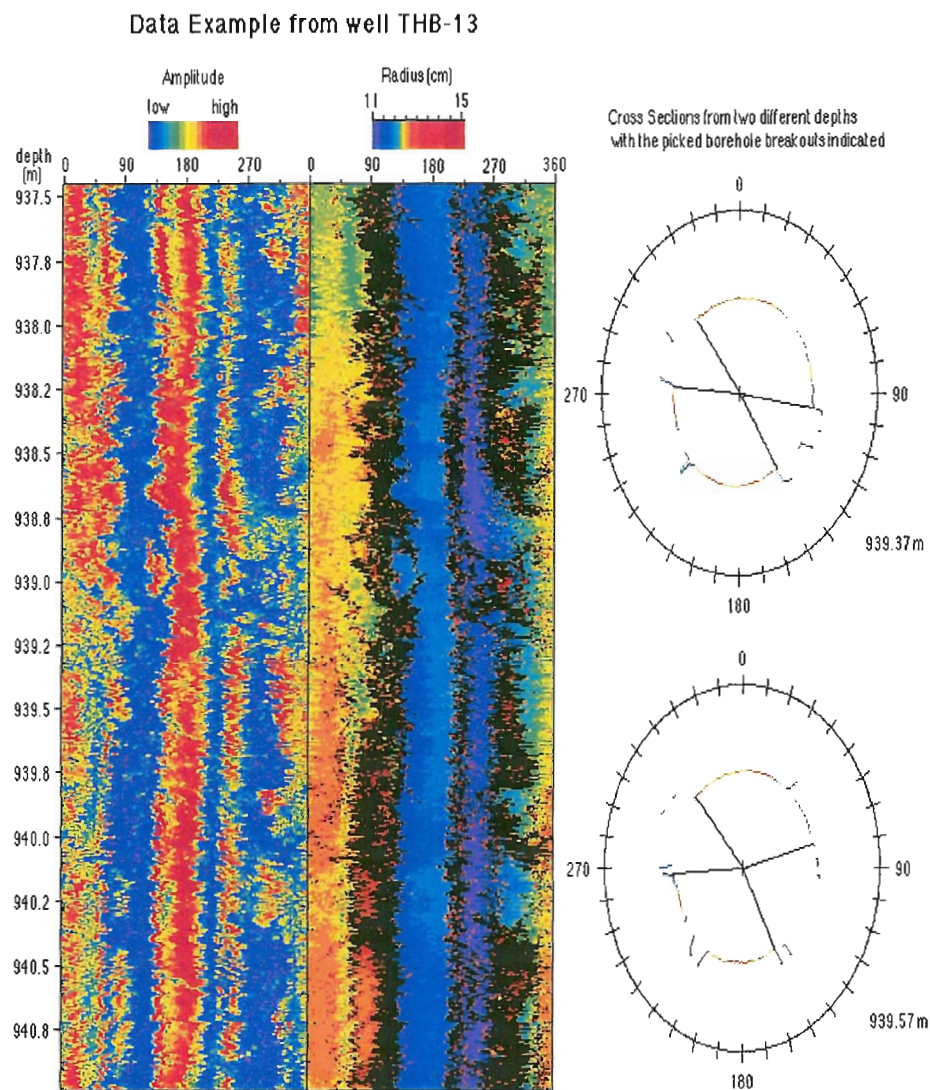


Figure 12. Example for the borehole breakouts found in Pykkvibær (THB 13) with two cross sections. The two panels show the amplitude of the reflected signal (left) and the radius calculated from the travel time (right), both unwrapped from N over E, S, W to N. Vertical axis: depth in meters. Breakouts appear as vertical bands of low reflection amplitudes. Due to low reflection amplitude, the values for the radius are often missing in these parts, resulting in black bands. In the two cross sections, the black lines indicate the range in azimuth of the picked breakouts.

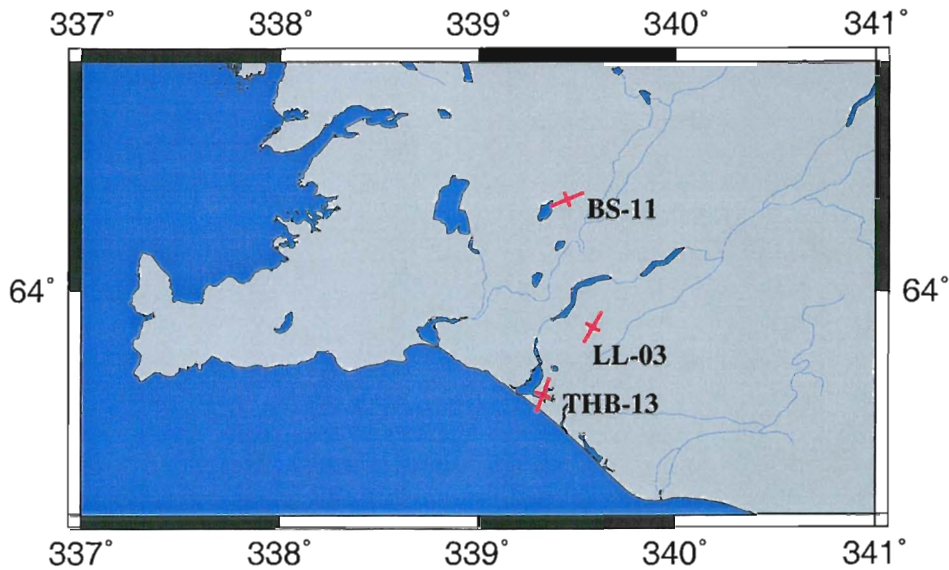


Figure 13. *Map of South Iceland showing the stress orientations found at Nefsholt, Þykkvibær and Böðmódsstaðir.*

## 5 Active deformation determined from GPS and SAR

### SAR interferometry study of the South Iceland seismic zone

The Hengill triple junction, at the western end of the South Iceland seismic zone (SISZ), exhibits the highest level of continuous seismicity in Iceland. In July 1994, an unusually persistent swarm of earthquakes, with magnitude less than 4, continued through 1995 with intermittent activity through 1999. This seismicity appears to be mechanically coupled to the ongoing volcanic activity. To study this coupling, we measure crustal deformation using interferometric analysis of synthetic aperture radar (INSAR) images acquired by the Earth Resources Satellites ERS-1 and ERS-2 of the European Space Agency. This technique provides dense ( $\sim 100$  pixels/km<sup>2</sup>) spatial coverage and monthly sampling in the summer months between 1993 and 1998. The resulting interference patterns show clear fringes, even after four years, on the barren ground cover near the Hengill central volcano. The radar coherence breaks down, however, in less than a month in the coastal lowlands containing most of the active faults of the SISZ. The principal signal in the interferograms is a concentric pattern with radius of approximately 10 km, centered on Hrómundartindur volcano. These fringes indicate a relative shortening of the radar line-of-sight distance (range) of approximately 1.5 cm/year. We interpret this signature as mostly vertical uplift due to increasing pressure in a magma chamber at depth. To explain it, we employ a simple "Mogi" model of a point source in an elastic half space. After estimating the four parameters of this model for each of the 10 observed interferograms, we find that the rate of uplift is constant, with an average value of  $19 \pm 2$  mm/year from 1993 through 1998.

The best fitting models locate the point source at a depth of  $7\pm 2$  km depth at  $64.032^\circ\text{N}$  and  $21.213^\circ\text{W}$ . The constant rate of volcanic deformation contrasts markedly with the episodic moment release by swarms or "crises" of earthquakes. To explain this contrast, we propose that the ongoing volcanic activity increases the stress in the brittle country rock. When the stress reaches the Coulomb failure threshold, the rock breaks, rupturing a fault and releasing the stress (Figure 14).

### GPS measurements of absolute displacements

The work planned in this subproject changed significantly in response to the enhanced earthquake activity at Hengill at the western end of the SISZ. Rather than operating one semi-continuous GPS station, we participated in the installation of 4 continuously recording GPS stations in the Hengill area as described in Section 1.

The planned static GPS measurements were also concentrated on the Hengill area. The static measurements have been conducted at regular intervals of few months since the beginning of the PRENLAB-2 project, and these show the continued expansion and uplift of the area of the enhanced earthquake activity [40].

PRENLAB-2 related work includes also static GPS measurements on the Reykjanes peninsula in 1998, that shows how left-lateral shear is continuously accumulating across the plate boundary in South Iceland [41]. A study has also been conducted on how to relate crustal uplift, to the volume of magma/gas accumulation at depth in the crust [42]. This is considerable of interest for the activity at Hengill, as one must understand how to relate the observed crustal deformation to changes that take place at deeper level in the crust, e.g. magma accumulation.

### Digitized fault map

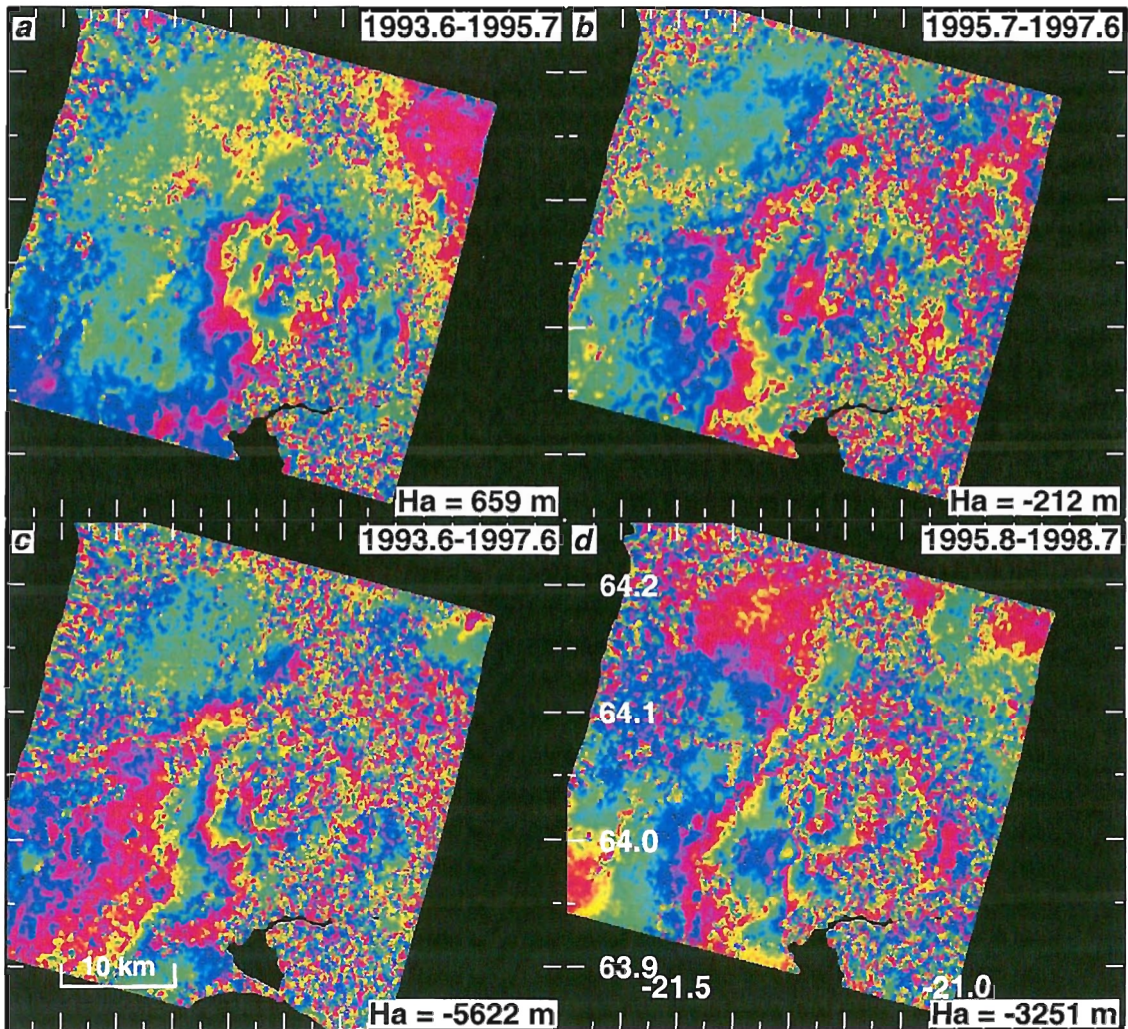
A digitized fault map of the South Iceland seismic zone is a prerequisite for a meaningful interpretation of deformations measured by SAR and GPS technology. Surface expressions of seismogenic faults of the area have been mapped in varying detail during the last two decades, most extensively by students in the Department of Geology and Geography of the University of Iceland. It was decided to gather this information and assemble a homogeneous map of the faults in digital form. This task was approached in two steps:

- Field work to fill in the largest gap in the area, the Holt district. This part of the seismic zone is covered with loose material such as glacial moraines and moors as opposed to postglacial lavas in most other parts. Surface faults and fractures are therefore poorly preserved. The structures found were mapped with differential GPS instruments at a scale of 1:1000.
- Systematic mapping of faults of the whole zone from aerial photographs at a scale of 1:50000 and digitizing of the maps.

### Achievements

- Structure of the active faults and fault systems. The active faults of the seismic zone are expressed at the surface by arrays of en-echelon fractures. The fractures themselves have a NNE to NE orientation. Most of the arrays, on the other hand, have a N to NNE orientation. The en-echelon arrangement is therefore left-stepping reflecting a large component of right-lateral horizontal shear movement along the arrays. Evidence for faulting along the conjugate direction, i.e. left-lateral slip on

# Hengill Area



28 mm per fringe

Figure 14. Four interferograms of the Hengill area. Radar images were acquired by the ERS-1 and ERS-2 satellites from ESA. a) Orbit numbers 10761 and 1953 from August 1993 and September 1995. b) Orbit numbers 1953 and 11973 from September 1995 and August 1997. c) Orbit numbers 10761 and 11973 from August 1993 and August 1997. d) Orbit numbers 2454 and 17985 from October 1995 and September 1998. One fringe in the interferogram represents 28 mm of range change. The main signal is a 10 km circular fringe pattern interpreted as an uplift of the area due to a pressure increase in a magmatic source at depth. The uplift rate is constant with time with a value of  $h_o/\Delta t = 1.9$  cm/year. In the four-year interferogram (c), up to 2 fringes are visible. The inferred uplift estimated from a Mogi model during this interval is 7.5 cm.

ENE striking faults, exists but is very rare. Individual fractures are either purely extensional or have a component of right-lateral movement. Push-up structures are frequently observed between the tips of adjacent fractures. These are hillocks of different size, ranging between a few centimeters in height to a few meters. They reflect horizontal compression in the direction of maximum compressive stress. The en-echelon arrangement of fractures can be seen on many scales within the same fracture system. Individual fractures ranging in length between 1 and 50 m may thus form an array 100-200 m long. The arrays may then be arranged en-echelon within a system on the scale of a kilometer. The kilometer sized systems may then again be arranged en-echelon to form a super-system of 10 km length. Description and maps of these structural relationships have been published in a series of papers [26, 27, 12, 30, 29].

- Surface ruptures of the earthquakes of 1630 and 1784 identified. Contemporary accounts of a large earthquake in the year 1630 mention ".. that large fissures were formed where there had been none before, in particular near the farm Minnivellir". These fractures have been mapped and found to belong to an extensive fracture system with the typical structures of the strike-slip faults of South Iceland. The system is more than 7 km long and has a N-S orientation.

The earthquake of August 14, 1784, is considered to be the largest historical earthquake in Iceland ( $M=7.1$ ). Its causative fault has been unknown except for the general area. Contemporary accounts mention that large fissures were formed in the northern part of the Holt district. The largest fractures found in this part of the seismic zone can be traced as a faint N-S system for a distance of 8 m. We assume that this is the expression of the 1784 causative fault.

Maps of the 1630 and 1784 faults are presented at the spring meeting of the Geoscience Society of Iceland [43] and will be published in a paper shortly.

- Digitized fault map. The compilation of fault data is in progress. About 3/4 of the area of the zone has been covered. Only the easternmost part is still to be done. This work has led to some new projects, including detailed mapping of faults around the towns of Selfoss and Hveragerði. The fault map of the South Iceland seismic zone will be published shortly with an accompanying paper.

## **6 Effects of stress fields and crustal fluids on the development and sealing of seismogenic faults**

### **Paleostress fields associated with the test areas from fault-slip data**

Within PRENLAB-2 there has been a focus on the analysis of fault slip data and the reconstruction of paleostress tensors on the Tjörnes fracture zone (TFZ)(Figure 11).

Detailed field observations in the Tjörnes fracture zone and elsewhere show that major fault zones consist of two main structural units: a fault core and a fault damage zone. The core, where most of the fault displacement is accommodated, consists mostly of breccia and cataclastite; for major zones, it is commonly up to a few tens of metres thick. On either side of the core is a damage zone, as much as several hundred meter thick. The damage zone includes numerous faults and fractures, many of which are filled with secondary minerals, but lacks large volumes of cataclastic rocks and breccia. A model is being developed where during the interseismic period of an active fault zone, the fault core

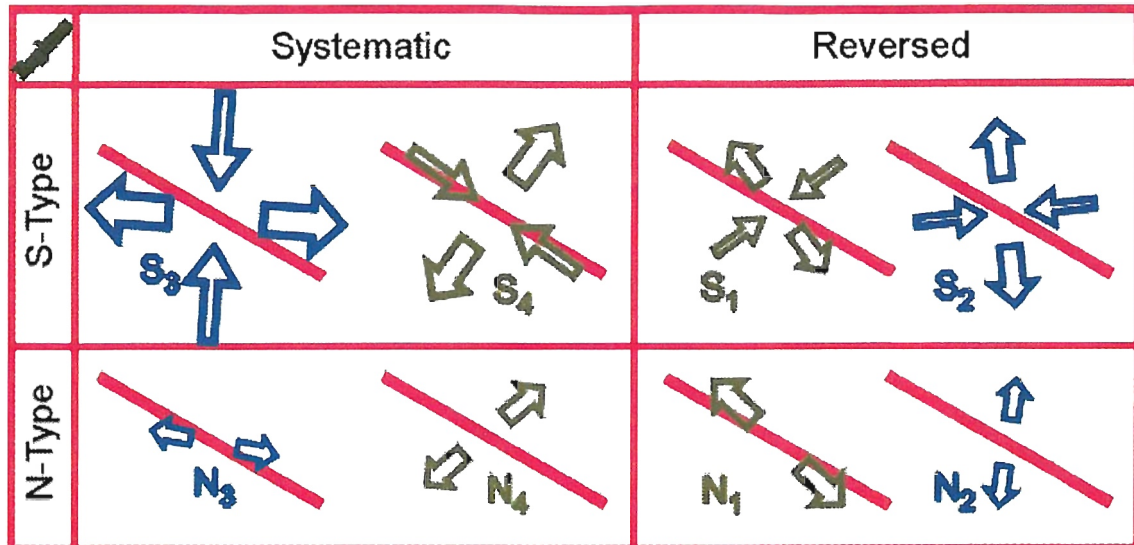


Figure 15. *Synthesis of results in terms of natures and orientations of the eight main tectonic regimes identified in Flateyjarskagi. Divergent arrows: average trends of extension (s3 axes), for S- and N-type regimes. Convergent arrows: average trends of compression (s1 axes), for S-type regimes. Thick line: N120°E trend of right-lateral transform fault zone.*

normally behaves as a porous medium with a very low hydraulic conductivity whereas the damage zone behaves as a parallel-fractured medium with a normal hydraulic conductivity many orders of a magnitude higher than that of the interseismic core.

Collection of more than 1300 fault slip data in 20 sites and determination of paleostress tensors in Flateyjarskagi in the Tjörnes fracture zone (Figure 17) allowed us to identify eight major brittle tectonic regimes (Figures 15 and 16) arbitrarily named S1, S2, S3 and S4 (strike slip in type) and N1, N2, N3 and N4 (normal in type). Frequent contradictions in this relative chronology data suggest that these tectonic states alternated in a complex manner. These eight regimes can be arranged two by two (normal and strike-slip regimes with a same direction of S3). They have not the same importance in terms of numbers of sites and data. The tectonic regimes S3, S4, N3 and N4 are widespread. The main couple, S3-N3, indicates a N95°E trending extension on average. The second couple, S4-N4, indicates a N35°E trending extension on average. The two other couples, less important, S1-N1 and S2-N2 are related to N130°E and N175°E trending extensions on average, respectively. For each couple, the relationships Si-Ni involves simple permutation s1/s2 (Figure 15).

Considering the geometrical relationships between the directions of two major groups. Each group contains dominating S-type and N-type regimes, consistent with right-lateral transform motion, but also minor S-type and N-type compatible with left-lateral motion. One group is constituted by S3-N3 and S2-N2, the other one by S4-N4 and S1-N1. The dominating couple S3-N3 shows an angle of 25° between the trend of extension (s3) and of the Flatey segment of the transform zone. This behaviour of the transform zone reflects moderate mechanical coupling. In contrast, the couple S4-N4 shows an angle of 85° between extension and the transform direction (Figure 16).

This behaviour of the transform zone indicates very low mechanical coupling. The reversed regimes (S1-N1 and S2-N2) have little expression except near the transform,

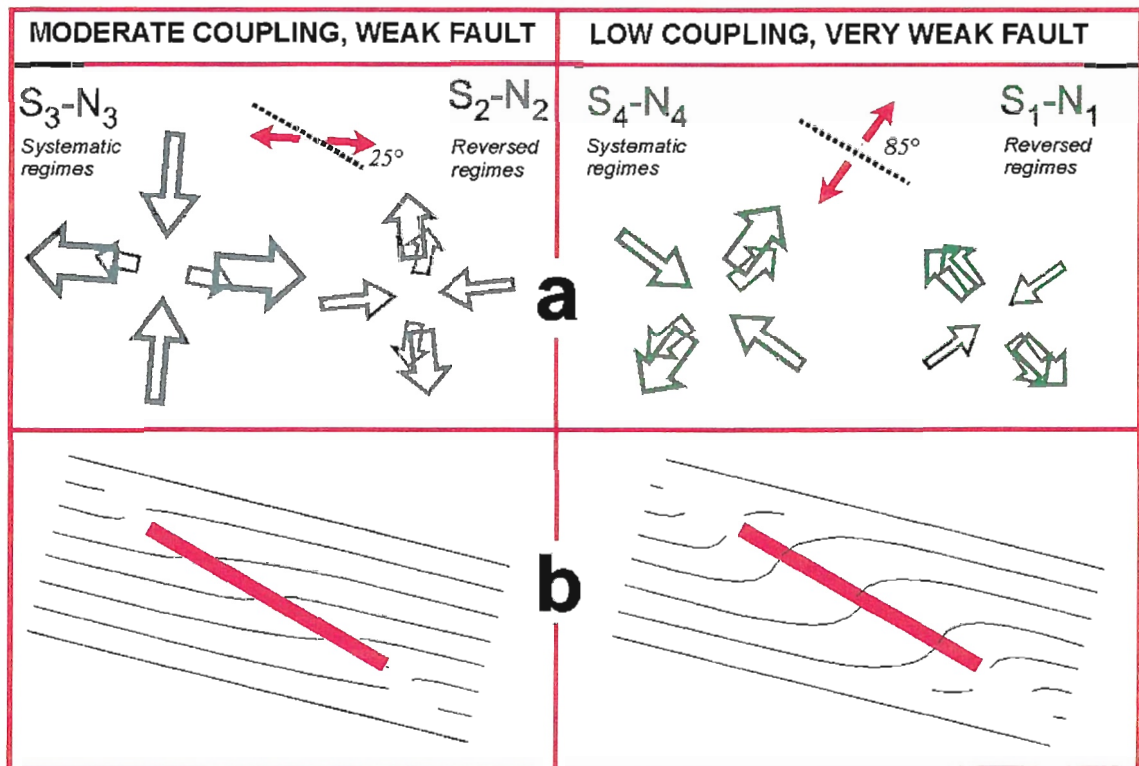


Figure 16. Interpretation of the Flateyjarskagi results, in terms of variable coupling near a transform zone. Moderate coupling on left, very low coupling on right. (a) groups of tectonic regimes. (b) schematic pattern of minimum stress trajectories (thin lines) around oblique transform fault zone (thick line).

where large deformation occurred. The drastic reversal  $s_1/s_3$  relative to the dominating stress regimes S3 and S4 and the minor ones S2 and S1, respectively, probably results from elastic rebound, fault block accommodation and magmatic injection phenomena. Variations in mechanical coupling across the Tjörnes fracture zone are the major source of the variations in the nature and orientation of tectonic regimes. Evidences for intermediate situations are few, suggesting that changes in coupling were abrupt rather than progressive [1, 10].

The work on the South Iceland seismic zone, carried out during the PRENLAB-1 project has been completed and some papers have been published [6, 7, 10]. A comparison between the geometrical patterns and the stress fields of the South Iceland seismic zone and the Tjörnes fracture zone has been carried out, based on the results obtained in the PRENLAB-1 and PRENLAB-2 projects [10].

### **Reconstruct the current stress fields associated with the test areas applying inversion of large sets of focal mechanisms of earthquakes**

We inverted of large population of earthquake focal mechanisms to derive the regional seismotectonic field. We studied a population of 48669 double-couple focal mechanisms of earthquakes, from 67717 events as evaluated by IMOR.DG during the years 1995 to 1997. Magnitudes range between -1.8 and 4.8. The purpose of this study was to determine whether such a large mass of data has the potential to indicate the general tectonic field. Many reasons suggested that this may be not the case: uncertainties of determinations, perturbations in tectonic regimes, and so on.

We considered two zones surrounding the major transform-rift zones north and south of Iceland: the Tjörnes quadrangle (66°-67°N, 16.5°-19.75°W) and the South Iceland seismic zone (SISZ) quadrangle (63.7°-64.25°N, 19.8°-21.1°W). Inversion was carried out based on a new direct method established during the PRENLAB-1 project, using 10547 and 4413 double-couple focal mechanisms in these two quadrangles respectively.

In both cases, the reconstructed  $s_2$  axes plunge 78° or steeper, indicating dominating strike-slip mode. The average direction of extension ( $s_3$  trend) is N66°E for the Tjörnes quadrangle and N143°E for the SISZ one. Selecting only the data fit significant quality requirements results in no or little change, with N66°E and N146°E trend respectively: 9831 and 1916 mechanisms are thus retained respectively. This stability of the inversion indicates that the results are significant. The ratio  $F$  between principal stress differences average 0.6-0.7, indicating that in terms of magnitudes,  $s_2$  is closer to  $s_1$  than to  $s_3$ . This is consistent with the association of normal and strike-slip faulting modes.

Considering the general trend of plate separation and related extension in Iceland, that is, N104°E, these results in the main zones where transform faulting occurs north and south of the Icelandic rift (right-lateral and left-lateral respectively) are of particular interest. To the north, the trend of average extension is deviated counterclockwise of 38°. To the south, it is deviated clockwise of 42°. These deviations are in perfect agreement with the pattern of transform motions between the segments of the North-Atlantic oceanic spreading axis [2, 3].

### **Geodetic analysis of present day crustal displacements**

The Tjörnes GPS Network (TGN) (Figure 17) consists of about 45 sites distributed in the northern Iceland seismic zone.

It completes the geodetic networks already installed over the whole Iceland at a smaller

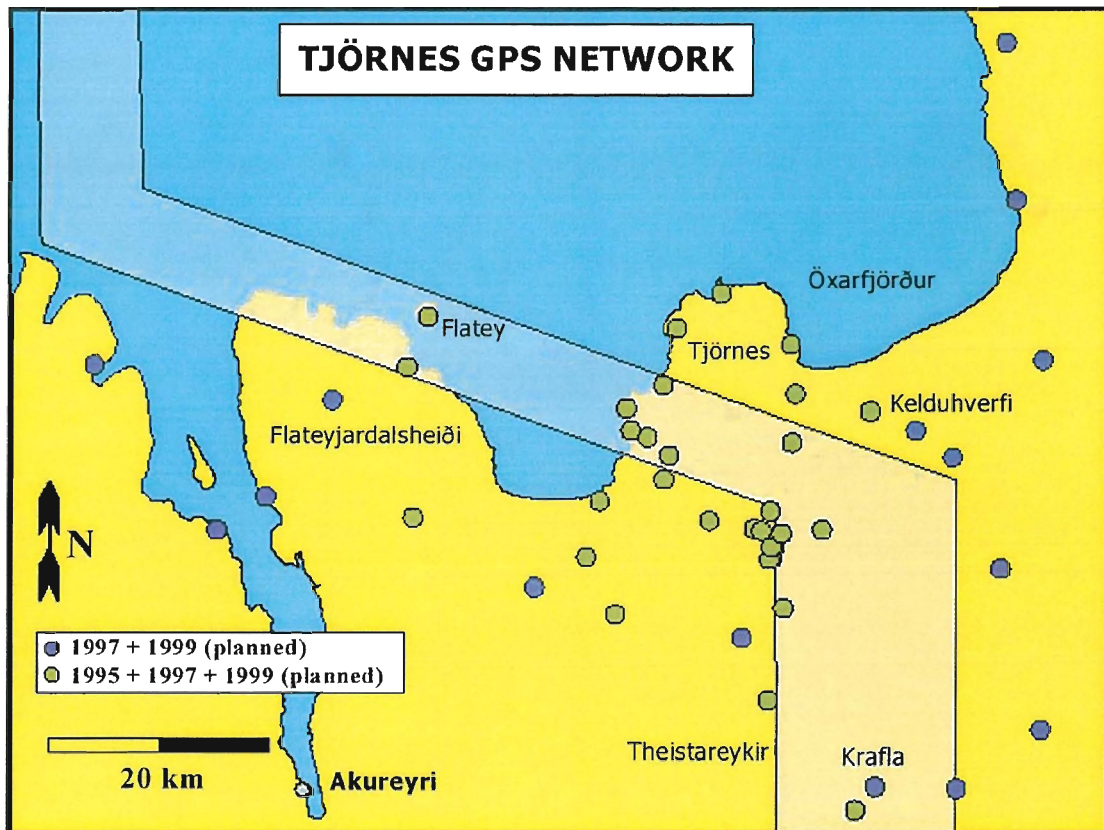


Figure 17. The Tjörnes GPS network in northern Iceland. The Húsavík-Flatey WNW-ESE transversal fault zone and its connection to the N-S oriented rift zones are shown.

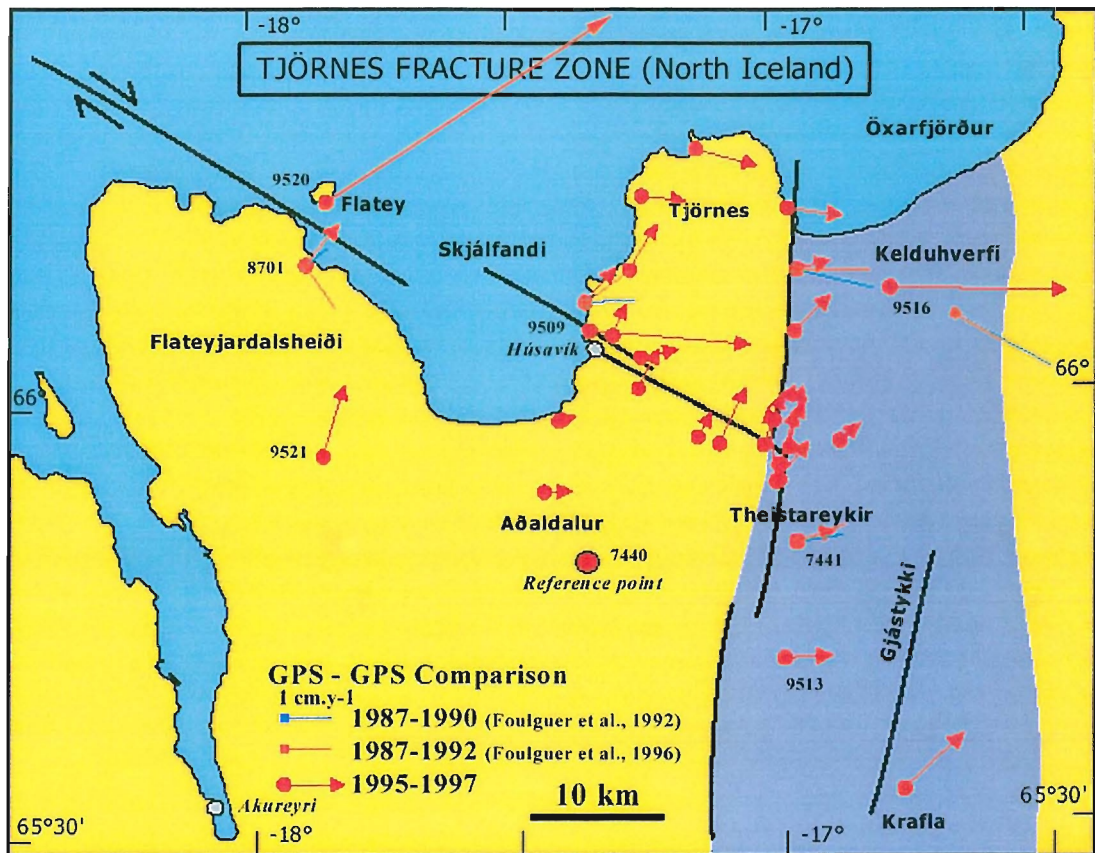


Figure 18. 1995-1997 displacements computed from GPS observations on the TGN network [44].

scale. The TGN has been designed to measure the surface displacement field on each side of the Húsavík-Flatey fault (HFF). It has been done in order to estimate if there are locked fault segments in the area and who these segments can contribute to increase the seismic risk. 32 points have been measured both in 1995 and 1997 [44].

The 1995-1997 velocities (Figure 18) have been computed by reference to a point located in the southern part of the network. All vectors are significant at a 95% confidence level [44]. Two tendencies can be distinguished on the Tjörnes peninsula: eastward velocities reaching 13 mm/year for the most northern points of the peninsula and NNE velocities up to 15 mm/year for the points located on both sides of the HFF. Displacements to the east have been computed for the points located in the fissure swarms. Points on Flateyjardalur move to the north. The point on the Flatey Island reveals a large displacement to the NE that could be due to a local instability. The assumption of an interseismic strain has been tested by using a simple dislocation model. This model assumes that a set of buried planar fault surfaces are locked above a given depth and affected by uniform aseismic creep below this depth. In order to determine this brittle/ductile transition we used the microseismicity recorded by the SIL network from 1995 to 1997. We assume that most earthquakes are localized in the brittle crust. Thus gives us a limit at a 10 km depth in average. We founded a solution that minimizes the differences between simulated and observed velocities [44].

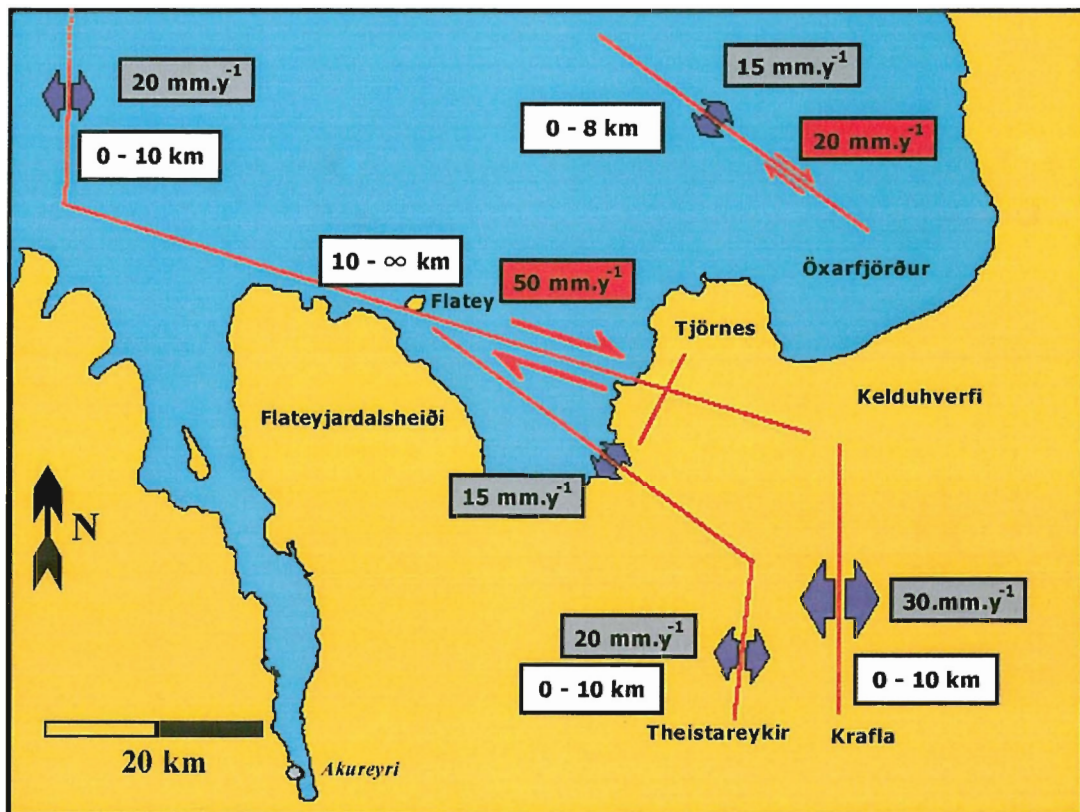


Figure 19. Model of fault pattern and present day activity for the transform zone in North Iceland. White boxes indicates the limit of the faults at depth; red boxes give the strike-slip velocity and pink boxes indicate the opening velocity for each fault [44].

The model (Figure 19) assumes: (1) a dyke opening of 20 mm/year affecting all the brittle crust along the Kolbeinsey ridge; (2) two dyke openings of 30 mm/year and 20 mm/year respectively along the Krafla and Peistareykir fissure swarms; (3) a dextral strike slip fault striking N100°E between the two previous rift segments with a velocity of 50 mm/year below a depth of 10 km and completely locked above the brittle/ductile transition; (4) a 15 mm/year opening zone striking N140°E south of the HFF; (5) a fault along the Grímsey lineament with both a 15 mm/year opening and 20 mm/year dextral strike-slip movements. In addition small wavelength tendencies has been adjusted by superficial faults. This model based on our 1995-1997 TGN comparison revealed extension and strike slip movements 3 to 4 times larger than the average velocity. The transform motion is locked on a large (150x10 km) fault surface and this represents the main risk for destructive earthquakes in the near future. From a mechanical point of view, the lockage could be due to the increase of normal stress on this surface following the double opening north and south of the fault zone.

### **Investigation of the potential effects of fluid pressure on the probability of faulting**

Studies of the aspect ratios of nearly 400 mineral-filled veins in the on-land parts of the Húsavík-Flatey fault on the Flateyjarskagi peninsula have been carried out. They indicate that the average fluid overpressure with reference to the minimum compressive principal stress, at the time of vein emplacement, was around 20 MPa [32]. In the current model on fluid transport along fault zones, it is proposed that during transport of overpressured fluids, such as are commonly associated with seismogenic faulting, the hydraulic conductivity of the damage zone can greatly increase. An overpressured fluid increases the apertures of the fractures constituting the network of the damage zone, and as a consequence the volumetric flow rate can, temporarily, be several hundred times greater than during fluid flow under hydrostatic pressure. Similarly, during periods of seismogenic faulting along the core, its hydraulic conductivity, and the associated transmissivity (conductivity times core thickness), may increase by many orders of a magnitude. As an example, a single fault plane along the core with an aperture of only 0.1-1 mm can transmit many hundred to many hundred thousand times more water than a porous fault core, tens of meter thick and with high values of hydraulic conductivity [33, 37]. This model may partly account for the great volumes of water that are commonly inferred or observed to be transported during seismic activity in large-scale fault zones. The locking of the Húsavík-Flatey fault as a result of dyke injection in the Krafla volcanic system in early 1976 has also been proposed, and that since this time the fault has been gradually unlocking, particularly after the M=5.5 earthquake in 1994 [36]. It has also been suggested that the 27 km long feeder dyke of the Laki 1783 eruption increased shear stress in the South Iceland seismic zone and almost certainly triggered the largest (M=7.1 in 1784) historical earthquake in that zone [36].

### **Detailed analysis of the Tjörnes fracture zone test site and its vicinity**

The Krafla fissure swarm (KFS) has been very active during the last rifting episode (1975-1984). This 80 km long and 10 km wide swarm includes numerous tension fractures and normal faults. Most of them has been reactivated during the last volcano-tectonic episode. Part of them elongated and we noticed the creation of new fissures. A complete mapping of the swarm before and after the rifting episode has been made from aerial photos [64].

If we assume that the deformation along a transverse section increases with the number of fractures encountered through the section we observe an evolution of the dilation along the swarm strike. This could be related to an unique dyke present at a small depth which controlled the surface fracturing [64]. A comparison between the two mapped states (1960 and 1990) permits us to distinguish between reactivated and new fractures. We assume that the growth process has not changed since the swarm created a limited number (<10) of tectonic episodes occurring on the KFS [64]. This implies that the volcanic episodes are not necessary associated with dilation along the whole swarm.

The Þeistareykir swarm (TFS) lies 20 km west of the Krafla fissure swarm and is connected with the transform zone in its northern end. A complete mapping of the fissure swarm has also been made from aerial photos. The western boundary faults consist in high scarps where both active normal and strike slip faulting has been characterized during the 1998 field trip. In addition displacement profiles has been measured by kinematic GPS on a set of 8 en-echelon normal faults just where the Húsavík fault meets the TFS. No clear evidence for a continuation at depth of the Húsavík lineament can be found on these profiles.

### **Analyzing the fracture properties of Icelandic rock in the laboratory and to make theoretical, observational and experimental studies on the sealing of seismogenic faults with application to the test areas in Iceland**

The main objective of this work was to determine the range of temperature, pressure and damage conditions in the crust under which rocks will fracture in a brittle-elastic manner. In order to achieve that objective, we have designed and constructed an apparatus for the measurement of rock fracture properties at high temperatures and pressures, and performed a series of experiments to measure rock fracture and fluid transport properties.

We have designed and manufactured an environmental cell for the measurement of fracture mechanics parameters under high-temperature/high-pressure conditions. The design conditions are: (i) confining pressure up to 70MPa, (ii) temperature up to 450°C, and (iii) water as the confining/pore fluid. Due to the highly corrosive nature water under these conditions, it was necessary to manufacture the cell and all its internal components from Hastalloy C (a high-strength nickel alloy developed by the US Navy). The cell has an outside diameter of 170 mm and an internal bore of 100 mm.

The cell is designed to take 60 mm diameter "short-rod" fracture mechanics specimens, manufactured to the standard ISRM geometry. Sample are heated by a fixed internal element, and are loaded to failure in tension by means of a small internal hydraulic actuator.

#### Starting material

Most of the measurements reported here were made on samples of a macroscopically isotropic basalt collected from a roadstone quarry located southeast of Reykjavík, Iceland. Microscopically it has an aphyric texture, comprising euhedral laths of unaltered plagioclase averaging 0.2 mm in length, and anhedral augite microphenocrysts averaging 0.1 mm in diameter, with accessory anhedral oxides up to 0.1 mm in diameter. No free quartz was visible under either optical or SEM microscopy.

#### Changes and evolution of rock physical properties with temperature

In order to better interpret results from experiments conducted at high temperatures, we have first made measurements at room temperature on samples that have previously

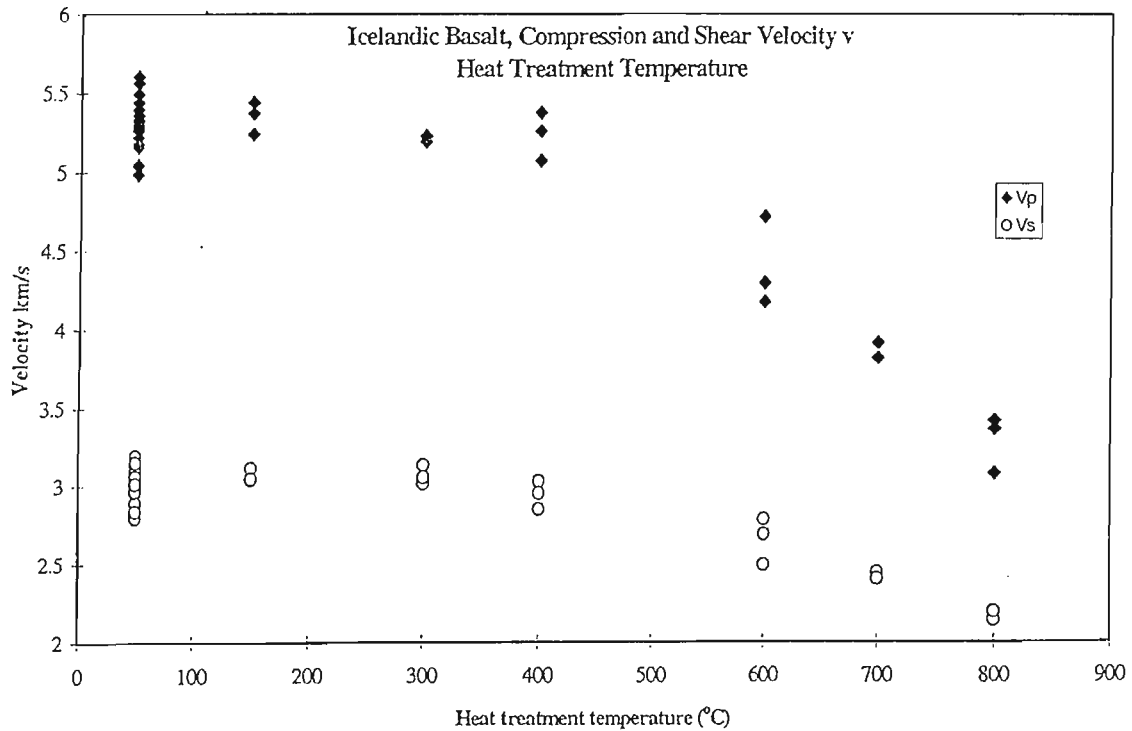


Figure 20. Variation in acoustic wave velocity with heat-treatment temperature.

been heat-treated to temperatures up to a maximum of 900°C in order to induce thermal crack damage. Thermal cracking can occur due both to thermal expansion mismatch between different mineral phases, and to thermal expansion anisotropy within a single mineral phase. In a shallow crustal environment where the geothermal gradient is anomalously high, such as in Iceland, thermal stresses may well be large enough to induce such fracturing. Furthermore, where enough fractures propagate and link up to provide an interconnected network, they can provide permeable pathways for fluid flow which can in turn lead to embrittlement and weakening of the rock.

All samples were heated in a tube furnace to the desired temperature at a controlled rate of 1°C/min, then held at that temperature for one hour, before cooling to ambient temperature at the same rate. This rate results in a temperature gradient across the sample of less than 1°C/cm, which is too low to cause any cracking due to thermal gradient stresses.

Thermal cracking in the basalt was monitored by measuring the compressional (P) and shear (S) wave velocities through the samples both prior to and following heat-treatment, and the results are shown in Figure 20.

Note that both P-wave and S-wave velocities remain essentially constant up to 400°C, with values of about 5.3 km/s and 3.0 km/s respectively. For higher temperatures the velocities decrease rapidly, so that by 800°C they have decreased to about 3.4 km/s and 2.2 km/s respectively.

#### Fracture toughness of heat-treated Icelandic basalt

We have also performed a series of fracture toughness measurements on heat-treated 60 mm diameter short-rod specimens of Icelandic basalt using the ISRM recommended

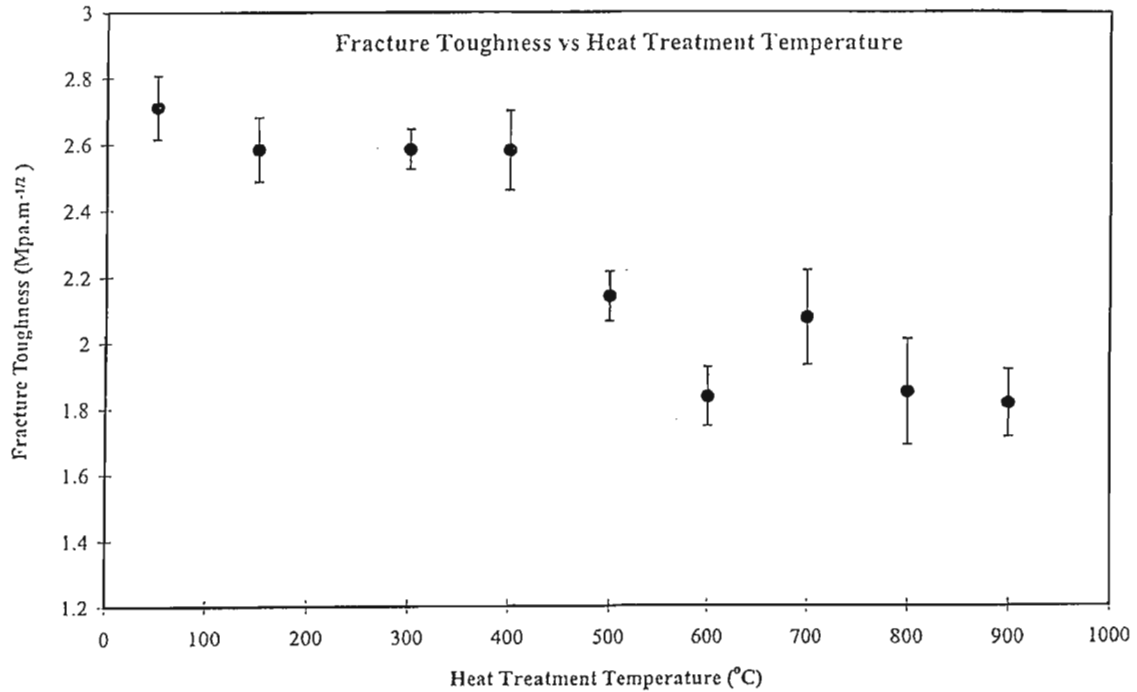


Figure 21. Variation in tensile fracture toughness for Icelandic basalt.

methodology. The results are presented in Figure 21.

The fracture toughness value of  $2.71 \text{ MPa}/\text{m}^{1/2}$  for the samples that were not heat-treated compares well with previously published data for very similar materials [47]. The fracture toughness remains essentially constant up to  $400^\circ\text{C}$ , but there is then a very rapid decrease in fracture resistance between  $400^\circ\text{C}$  and  $600^\circ\text{C}$ , with relatively little change between  $600^\circ\text{C}$  and the highest heat-treatment temperature of  $900^\circ\text{C}$ . This pattern of behaviour is entirely consistent with the wave velocity data. These experiments were conducted in air with rapid loading, so that environmentally-assisted subcritical crack growth was not a significant factor. Any reduction of fracture resistance must, therefore, be due to changes in the microstructure of the rock due to thermal cracking.

We have observed very similar trends in measurements of the indirect Brazilian tensile strength and Young's modulus for heat-treated basalt samples. These other results are not reported here due to space constraints.

#### Crack linkage and enhanced fluid permeability in heat-treated Icelandic basalt

In these experiments, the fluid permeability of basalt samples 40 mm in diameter by 40 mm in length were measured both prior to and following heat-treatment. All permeability measurements were carried out using a new wide-range permeameter system that makes use of two servo-controlled fluid pressure intensifiers to enable permeabilities from 1 darcy to lower than 1 nanodarcy to be measured, using water as the pore fluid. The mean permeability of the basalt prior to heat-treatment ( $k_0$ ) was 9.4 nanodarcy ( $9.4 \cdot 10^{-21} \text{m}^2$ ), and the change in normalized permeability ( $k/k_0$ ) as a function of heat-treatment temperature is plotted on Figure 22.

Similar to the previous results, the normalized permeability remained essentially constant after heat treatment to temperatures up to  $300^\circ\text{C}$ , and showed only a slight increase

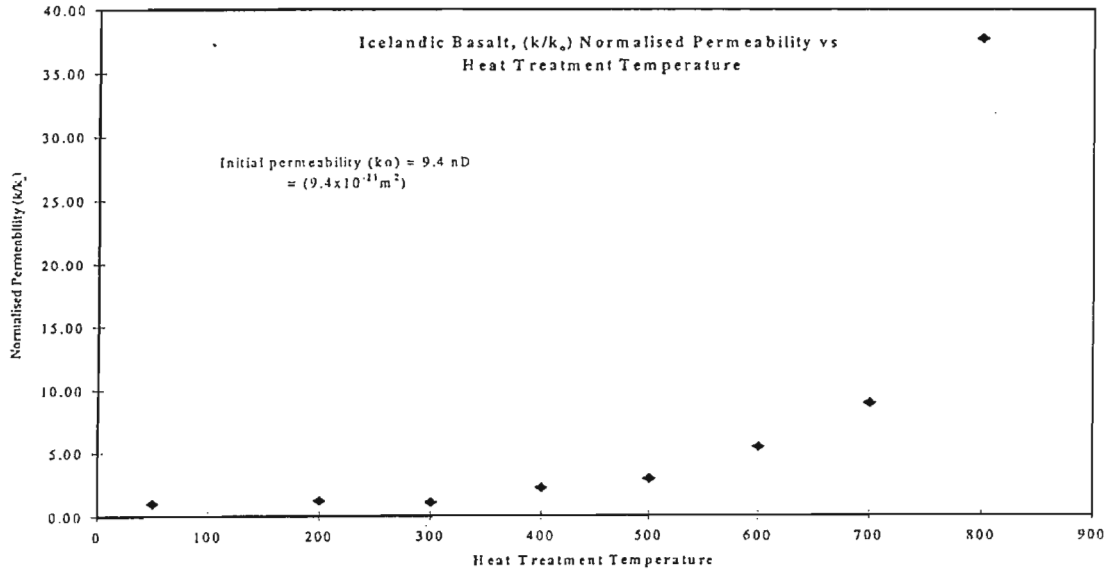


Figure 22. Increase in basalt permeability as a function of heat-treatment temperature.

after treatment to 400°C. At higher temperatures, however, the normalized permeability changed dramatically, increasing by an order of magnitude at 700°C and by a factor of 40 by 800°C.

It is clear that such a large increase in permeability is unlikely to result merely from the increase in the number or size of thermally-induced cracks. Note, for example that over the same temperature interval the rock strength (as measured by fracture toughness and Brazilian tensile strength) decreased by only about 30%. We believe, therefore, that these permeability results show the profound effect of crack linkage processes above some percolation threshold to form extensive sample-spanning permeable pathways for fluid flow.

Due to the high temperature gradient and low lithostatic stress, thermal cracking may be an important process in controlling fracture in Icelandic crust. In the absence of confining stress, such cracking starts in the temperature range 300°C to 400°C in fresh basalt. This leads to significant decrease in mechanical strength and resistance to crack propagation at higher temperatures. Thermal cracking also leads to increased fluid permeability above about 300°C, with the permeability increasing very non-linearly with temperature. The decrease observed in rock strength is likely to be considerably enhanced by the presence of a chemically active pore fluid (e.g. water), especially when its activity is increased by elevated temperatures.

In the next phase of the project, we will measure the same key parameters under elevated temperature and pressure, and modify our experimental apparatus for the measurement of compressional and extensional strength.

## 7 Theoretical analysis of faulting and earthquake processes

### 7a Ridge-fault interaction in Iceland employing crack models in heterogeneous media

#### Magma upwelling as driving mechanism for the stress build-up in the elastic lithosphere

Tensile cracks are often employed to model magma migration in rift zones or within volcanic edifices, through lateral or feeding dykes. In a crack model, the overpressure of magma  $\Delta p$  with respect to the horizontal stress in the host rock, is assumed to be responsible for dyke opening and propagation. Most crack models of dykes have been developed so far in homogeneous media. The most simple heterogeneous medium has been considered, made up of two welded half-spaces, characterized by different elastic parameters. The analytical solutions available for the elementary dislocation problem in such a medium [13] has been employed to set up an integral equation with generalized Cauchy kernel, representing the condition for static equilibrium. The unknown in such a problem is the dislocation density distribution, whose singular behaviour has been studied near the crack tips and near the intersection with the interface between the two media. When the crack is in half-space 1 but touches the interface, the order of singularity of the dislocation density distribution at the interface changes from the classical behaviour  $\sim r^{-1/2}$  to  $\sim r^{-b}$  (where  $r$  is the distance from the interface) and the order of infinity  $b$  is obtained solving a transcendental compatibility equation; some results are shown in Table 3.

$m = \mu_1/\mu_2$	$\infty$	10	5	2	1	0.5	0.2	$10^{-1}$
$b$	0.255	0.312	0.352	0.430	0.500	0.576	0.678	0.752

Table 3. *Crack touching the interface.*

A crack crossing the interface  $z = 0$  between the two half-spaces with rigidities  $\mu_1$  (in  $z > 0$ ) and  $\mu_2$  (in  $z < 0$ ) has been considered in detail. A system of generalized Cauchy equations is obtained, which is solved for the dislocation density distributions of each crack section. An internal singularity in the dislocation density distribution appears at the intersection between the crack plane and the interface. This singularity is again of the type  $r^{-b}$  on both sides of the interface and its order  $b$  depends only upon the elastic parameters of the media in welded contact and the ratio between the crack lengths in the two half-spaces (see Table 4). More specifically, the order  $b$  does not depend on the stress drop.

$m = \mu_2/\mu_1$	1	0.5	0.1	0.05	0.001
$b$	0	0.030	0.170	0.208	0.245

Table 4. *Crack crossing the interface.*

Crack induced stress components are plotted in Figure 23, assuming a 5 MPa overpressure within the crack. From a comparison with solutions pertinent to a homogeneous medium, it appears that layering can be responsible of stress changes, localized along the the interface, which may be considerably higher than the overpressure within the dyke. These results provide useful hints for the interpretation of induced seismicity in rift zones and in volcanic areas. [14]

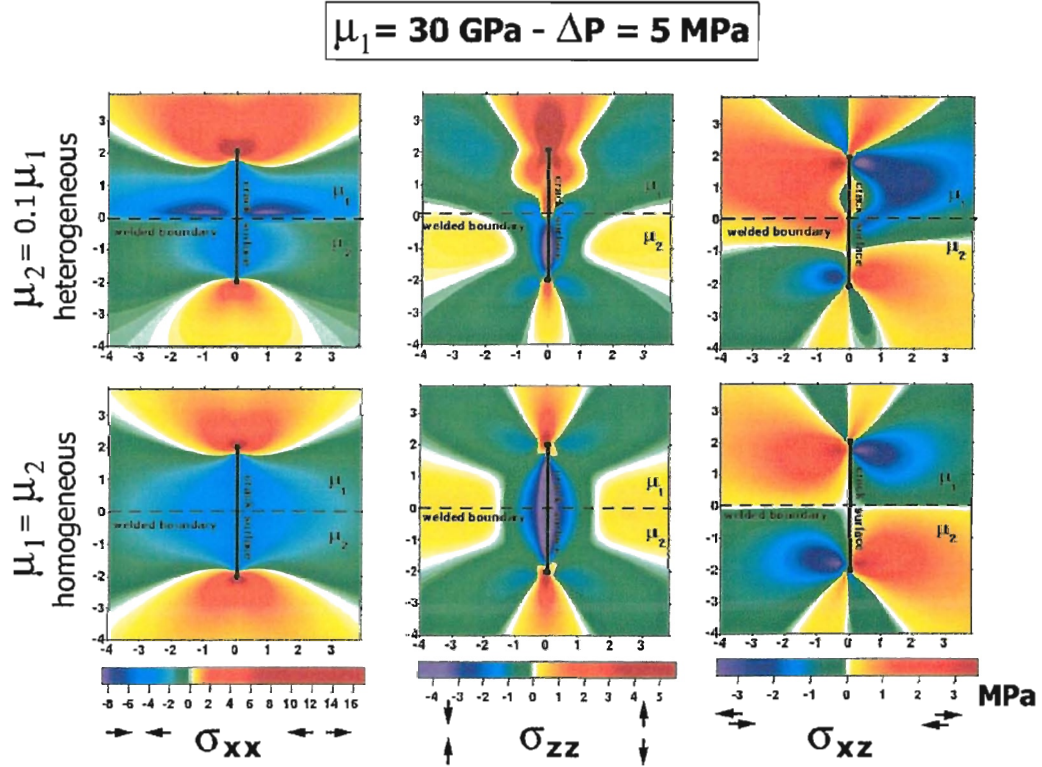


Figure 23. *Stress components induced by rifting in proximity of a structural discontinuity.*

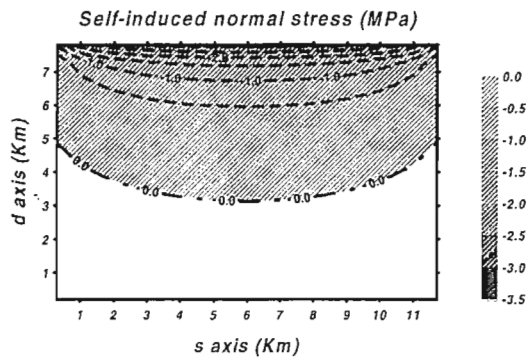
### Space-time evolution of the stress field following earthquakes and episodes of magma upwelling

Mechanical effects left by an earthquake on its fault plane, in the post-seismic phase, are investigated employing the "displacement discontinuity method" and imposing the release of a constant, uni-directional shear traction. Due to unsymmetric interaction between the fault plane and the free surface, significant normal stress components are left over the shallow portion of the fault surface after the earthquake (Figure 24) these are compressive for normal faults, tensile for thrust faults, and are typically comparable to the stress drop.

In Figure 24 the  $s$ -axis is along the strike of the fault, the  $d$ -axis is along the dip (positive upwards). Several observations can be explained from the present model: low-dip thrust faults and high-dip normal faults are found to be favoured, according to the Coulomb failure criterion, in repetitive earthquake cycles; the shape of dip-slip faults near the surface is predicted to be upward-concave; the shallow aftershock activity commonly observed in the hanging block of a thrust event is easily explained. Detailed results are reported in [15].

Effects of structural inhomogeneities on the stress and displacement fields induced by strike-slip faults in layered media is presently under study. An elastic medium is considered, made up of an upper layer bounded by a free surface and welded to a lower half-space characterized by different elastic parameters. The case of a strike-slip fault crossing the interface between two elastic media is particularly interesting. The dislocation density distribution is found to be affected by a jump discontinuity at the interface, which is responsible for inducing high concentrations of deviatoric stress, not only in proximity of

Normal fault:  
dip angle 70 deg, stress drop 2.5 MPa, depth 0 Km



Thrust fault:  
dip angle 30 deg, stress drop 2.5 MPa, depth 0 Km

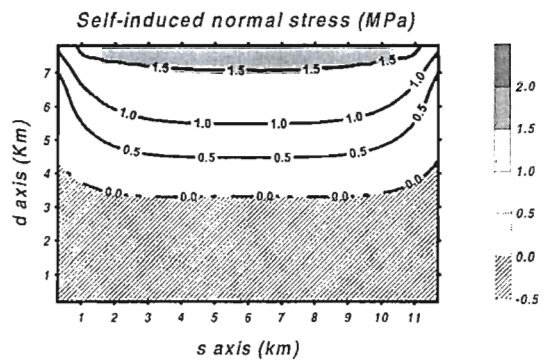


Figure 24. Normal stress induced by uniform stress drop over a high-dip normal fault and a low-dip thrust fault.

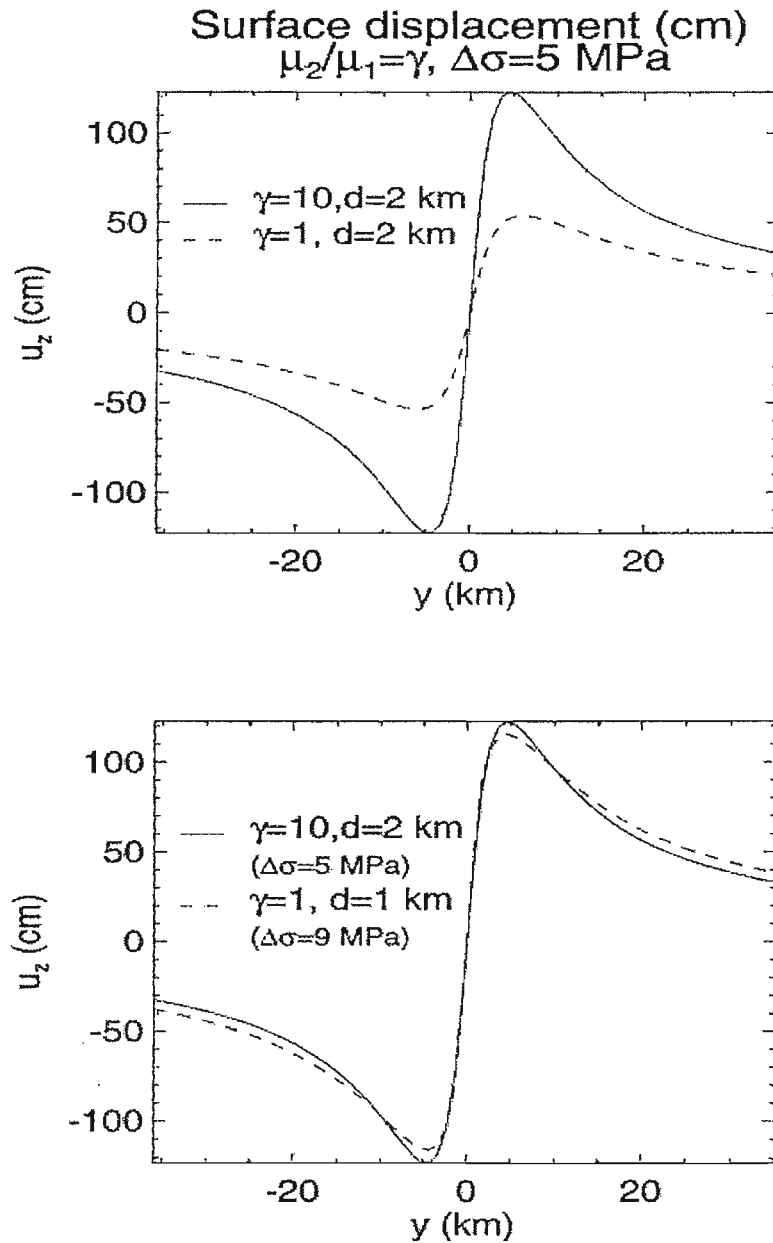


Figure 25. *Displacement at the free surface after a strike-slip event with uniform stress drop: layered half-space solutions are shown as solid lines, homogeneous half-space solutions as dashed lines.*

fault edges, but also along the interface where it may be even higher than the stress drop on the fault plane. The displacement field observable over the ground surface (Figure 25) is found to be strongly affected by the presence of a soft sedimentary layer (with rigidity  $\mu_2 \ll \mu_1$ ).

In Figure 25 the solid line shows the surface displacement induced by strike-slip faulting at depth greater than  $d = 2 \text{ km}$ , computed in the heterogeneous medium, the dashed

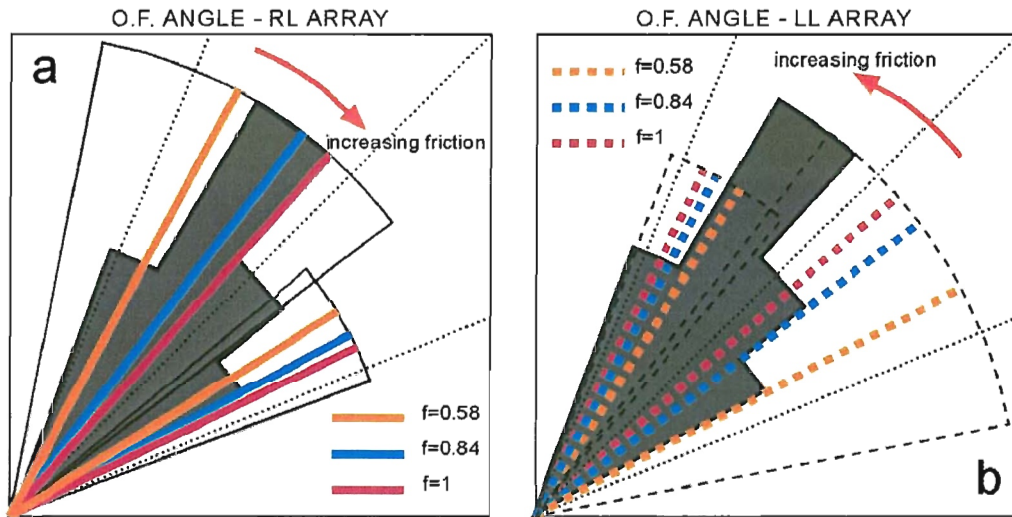


Figure 26. *Open fractures (O.F.) angles predicted from the combined effect of the main fault rupture and secondary fault (S.F.) rupture along the strike direction. The observed range and relative frequency of O.F. angles is shown shaded [12]. If the friction coefficient  $f$  varies between 0.2 and 1.5 predicted O.F. angles vary within the circular sectors contoured in black. Solid lines in panel (a) represent the angle expected for O.F. belonging to dextral arrays. Dashed lines in panel (b) represents the angle expected for O.F. belonging to sinistral arrays. In both panels, longer lines indicate the predicted mixed-mode O.F. trends, while shorter lines indicate pure tensile trends. Mixed-mode O.F. are assumed to share the same style of faulting (sinistral or dextral) with the array to which they belong. The dotted lines indicate 22.5°, 45°, 67.5° directions (for reference). Coloured lines refer to particular friction values (indicated). Friction increases as indicated by the red arrow.*

line show computation in a homogeneous half-space. It appears from panel (b) that estimates of  $d$  and  $\Delta\sigma$  derived from geodetic observations can be severely biased if structural heterogeneities are not taken into account. A paper is in preparation.

### Secondary earthquake fractures generated by a strike-slip fault in the South Iceland seismic zone

This task was included in the PRENLAB-1 workprogramme and was not originally included within the PRENLAB-2 workprogramme. The latest developments of this topic, however, lead us to include the main results in the present report. Most earthquakes in the South Iceland seismic zone occur on N-S trending dextral strike-slip faults. The resulting rupture zones display complex en-echelon patterns of secondary structures including NNE-trending arrays of (mostly) NE-trending open fractures (O.F.) and hillocks.

Three spatial scales characterize the surface faulting pattern: the length of the main fault (M.F.  $\sim 104$  m), the arrays here interpreted as surface evidence of secondary faults ( $\sim 102$  m) and the individual O.F. ( $\sim 10$  m). In order to improve our understanding of the genetic relationship between the O.F. and the M.F. we computed the stress field induced by slip on a buried M.F. using a dislocation model in a layered half-space: the fault surface

is assumed to be embedded in the basement rock, topped by a softer near-surface layer. The O.F. were preliminarily considered as pure mode-I cracks opening in the near surface layer in the direction of the maximum (tensile) principal stress. Alternatively, secondary fractures were interpreted, as mixed-mode cracks, slipping at depth as shear cracks and opening near the surface due to low confining pressure. The Coulomb failure function after the earthquake (obtained summing the M.F. stress change and the lithostatic stress) suggests that secondary faulting (S.F.) can be expected to occur in response to the main rupture below the upper soft layer down to few hundreds of meter depth. The total stress change induced by the M.F. and the S.F. (of smaller scale) is shown to yield quantitative explanations of the complex geometry observed in the fault region in terms of simple frictional laws and friction coefficients very close to those measured in the lab (Figure 26). Detailed results are reported in [5].

## **7b Modelling of the earthquake related space–time behaviour of the stress field in the fault system of southern Iceland**

The work described here is a direct continuation of work carried out during the last part of PRENLAB-1, to obtain forward models of the stress field and stress changes in the South Iceland seismic zone (SISZ).

The target is to model the space–time development of the stress field using data on strain and stress changes from the other experiments and from databases.

Two models were prepared during PRENLAB-1:

- A model of the South Iceland seismic zone and the adjacent part of the eastern volcanic zone.
- A scheme comprising the main ridge parts on Iceland and the North Atlantic ridge to the north and to the south of the island, including both faults and the load due to Katla and Hekla volcanoes.

It was modelled:

- The changes in crustal strain and stress due to earthquakes and aseismic movement in the fault system of the South Iceland seismic zone.
- The interaction of faults.
- The mutual influence between volcanic and earthquake activity, e.g. magmatic upwelling and shearing at fault zones.

### **The model for the earthquake sequence at the SISZ**

The main features of the model applied in PRENLAB-1 are described here to ease comparison with the new results:

#### **The method**

The forward modelling of stress fields is done by applying static dislocation theory to geodetic data and data obtained through the seismic moments from seismograms. It allows to calculate displacements, strain and stresses due to double-couple and extensional

sources in layered elastic and inelastic earth structures. Besides the change in displacement during the event, the changes caused by the movement of plates are included (for further details see e.g. [49]).

Usually, for earthquake hazard estimation, the location, magnitude and statistically estimated recurrence period of former events is used. To improve this, here the rupture length and width as well as the tectonic setting and the crustal deformation rates are considered while calculating the space-time development of the stress field.

### The targets

In general, with these models, the subproject aims:

- To achieve a better understanding of the distribution of seismicity in space and time, its clustering and migration in Iceland.
- To provide models for the joint interpretation of the data gathered in the whole research programme, of which this is one part.
- To compare models of stress fields at SISZ to those for stress fields in other regions, e.g. the North Anatolian fault zone.
- To make a contribution to the intermediate-term earthquake prediction in this populated and economically important region of Iceland.

### The tectonic setting

The SISZ is situated between two sections of the mid-Atlantic ridge, the Reykjanes ridge (RR) and the eastern volcanic zone (EVZ). Even though the angle between the SISZ and the neighbouring ridges is far from  $90^\circ$ , it is considered as a transform fault. Following the transform fault hypothesis, left-lateral shear stress is expected along the E-W striking zone. This is equivalent to right-lateral shear stress with N-S orientation. In fact, earthquakes seem to occur on N-S trending en-echelon faults ( [26, 38] and further references there). They are located side by side between the Hengill triple junction, where the RR meets the low activity western volcanic zone (WVZ) and Hekla volcano, a part of the EVZ [26] (Figure 27). As we further know from Sections 4 and 5, the orientation of the larger horizontal principal stress is NE-SW, i.e. fits to an active N-S or E-W trending fault, which is not a weak fault like the San Andreas fault, and the stress orientation seems to be constant since Pliocene time.

In detail, the questions to be solved are:

- Do these events, placed on parallel faults, release all the energy stored in the 3-D volume of the SISZ?
- Do the earthquakes always take place in areas of high stress?
- What is the critical stress level? How large is its variability?
- Where are the highest stresses nowadays?

The area investigated extends from  $18$  to  $24^\circ\text{W}$  and from  $63$  to  $65^\circ\text{N}$ . The origin is set to  $24^\circ\text{W}$ ,  $64^\circ\text{N}$  (cf. Figure 28) it includes the SISZ,  $\pm 1^\circ$  north and south of  $64^\circ\text{N}$ , the SW edge of the EVZ, and the north eastern most part of RR.

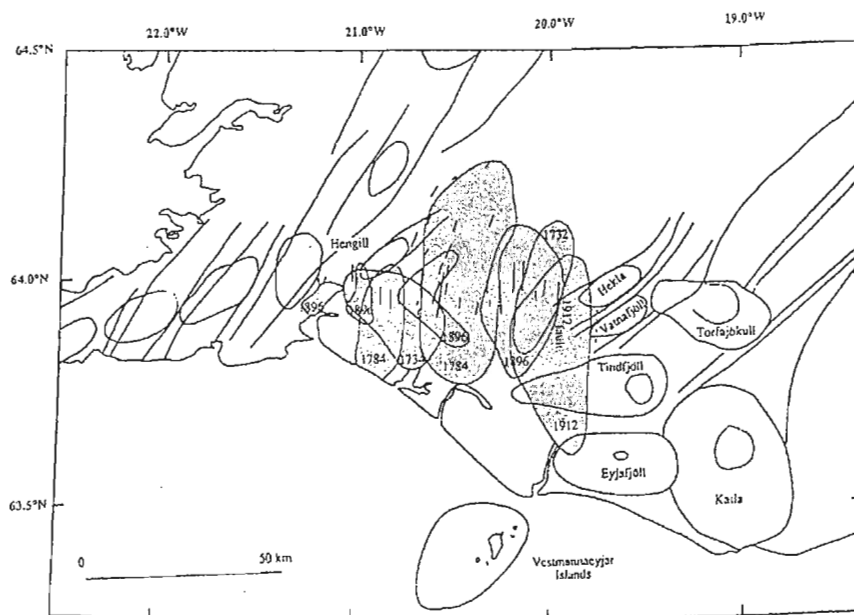


Figure 27. The South Iceland seismic zone showing mapped surface breaks and regions in which over half of the buildings were destroyed in historic seismic events [26]. The N-S dashed line near Vatnafjöll indicates the estimated location of the fault on which the May 25, 1987, earthquake occurred [11]. For the structural features and the coastline see [28].

### The initial stress field

The initial stress field is determined as follows: A tensional stress acting N103°E (nearly parallel to the SISZ [24]) is assumed, due to ridge push or basal drag of the adjacent plates. This rifting induces shear stresses in the region of the transform fault. The stress magnitude, which is unknown, is set to a value that produces left-lateral shear stresses in E-W direction as large as the stress drop determined for the largest event ( $M=7.1$ ) in the studied earthquake sequence.

Tensional stresses at both ridges are modelled as constantly being released to have zero values at the rifts. These are the major disturbances of the unknown background stresses.

On this initial field, the stress changes due to earthquakes are iteratively superposed as well as the stress changes due to further spreading at the ridge segments based on an opening of 2 cm/year. This value is taken from [24]. As the simplest assumption, lacking other data, the spreading rate is taken to be constant during the modelled time period, even though this can be questioned as for instance the present debate on the stress increase in the New Madrid seismic zone shows.

The stress field before every event is thus the sum of the initial field, the stress drop of all preceding events, and the plate tectonic stress build-up since the starting time of the model, which is set to 1706, when the first event in the series occurred.

Results were calculated for 56x44 test-points covering 280 km in E-W direction and 220 km in N-S direction. Stresses were computed for a homogeneous half-space, as a starting model. Although surface stress changes are calculated, these should be representative for crustal stresses using values for the moduli, that are typical for oceanic crust [25] and not for sedimentary layers at the surface.

Date <sup>1</sup>	Magnitude <sup>1</sup>	Epicenter <sup>1</sup>		South end of rupture <sup>2</sup>		Co-seismic slip <sup>3</sup> $U_0$ [m]	Rupture length <sup>4</sup> $L$ [km]
		Lat. °N	Long. °W	$x$ [km]	$y$ [km]		
1706	6.0	64.0	21.2	131	-5	0.30	10
1732	6.7	64.0	20.1	183	-11	0.77	22
1734	6.8	63.9	20.8	150	-23	0.96	25
14.08.1784	7.1	64.0	20.5	164	-18	1.9	35
16.08.1784	6.7	63.9	20.9	145	-22	0.77	22
26.08.1896	6.9	64.0	20.2	178	-14	1.2	28
27.08.1896	6.7	64.0	20.1	183	-11	0.77	22
05.09.1896	6.0	63.9	21.0	140	-16	0.30	10
05.09.1896	6.5	64.0	20.6	159	-9	0.48	18
06.09.1896	6.0	63.9	21.2	131	-16	0.30	10
06.05.1912	7.0	63.9	20.0	187	-27	1.5	32

Table 5. Earthquakes  $M \geq 6$  since 1706 in the South Iceland seismic zone. 1) Data taken from [60]. 2) Position in the model coordinate system with origin at 64° N, 24° W. 3) Calculated via the magnitude moment relationship  $\log M_0$  [dyne cm] =  $1.5M_S - (11.8 - \log(\sigma_a/\mu))$  with the apparent stress  $\sigma_a = 150$  MPa and the shear modulus  $\mu = 0.39 \cdot 10^{11}$  Pa [45], followed by using the values of  $\mu$  above, the rupture length as given in the table as well as a vertical fault width of 14 km east of 21° W and 7 km between 21° W and 21.2° W. Finally, the values were reduced by a factor of 2, following the discussion in [38]. 4) Calculated using  $\log L$  [km] =  $0.5M - 2$  [48] which results in slightly lower values compared to e.g. [55].

### The earthquake data

All events with  $M \geq 6$  since 1706 were used (Table 5) [38, 39, 59, 60]. The catalogue is supposed to be complete from 1706 for these earthquakes.

All ruptures were set to be oriented N-S, according to the isolines of damage intensity and surface ruptures shown in Figure 27. As only the 1912 event was instrumentally recorded, the source parameters are not very accurate – a problem to be discussed further below.

### **Changes and improvements in PRENLAB-2**

In the first phase of PRENLAB-2, the models developed in PRENLAB-1 were improved:

- A At the western end of the SISZ, segments with aseismic oblique slip (mainly normal faulting with a smaller component of left-lateral strike-slip) were introduced, to better fit the Reykjanes ridge (RR) between the SW tip of the Reykjanes peninsula to Hengill triple junction (Figure 28).
- B The test-point density was increased from 56x44 (5 km distance) to 280x220 (1 km distance) to get more details of the stress field and to reduce interpolation errors.
- C A layered model, including an inelastic asthenosphere below a brittle seismogenic upper layer, is in preparation.
- D To investigate the model resolution a set of different models is produced. Besides the main model, several extreme cases are assumed and the variation of the main results under these assumptions is observed.
- E The stress field at 1912, the end of the series of strong events with  $M \geq 6$ , is extrapolated to April 1999.

Concerning item A, the RR on Iceland is treated now completely as a zone of aseismic rifting, consisting of 2 sections with changing rifting and strike-slip components to model the bend of the ridge from SW towards the Hengill triple junction, as displayed in Figure 28. Doing so, not only the geometry of the rift is better fitted, but also stress build-up by plate motion is concentrated in the west near the Hengill triple junction instead of farther west in the RR. Now, seismic slip is confined to the SISZ ((125, -5) — (250, 0)), where the series of strong earthquakes simulated here, took place.

This model was calculated with a test-point spacing of only 1 km (item B). It will be named "improved model" below.

A selection of the results obtained by this model is given in Figures 29, 30, and 31. Figure 29 gives the initial stress field again with the dark red areas subject to the highest shear stress, now at the rift tip east of Hengill.

The pre-seismic stress level is expected to be smoother than before with the wider spacing of the test-points. As – at the same change, however – the high stress tip of the SISZ was shifted to Hengill, the westernmost events (1706, 1784b, 1896c and e) got into a higher stress region. This produces a larger scatter of the pre-event stress level, cf. Figure 31. However, the stress level for the main events remains in a similar range as before (between 2.0 and 2.8, now between 1.7 and 2.9 MPa).

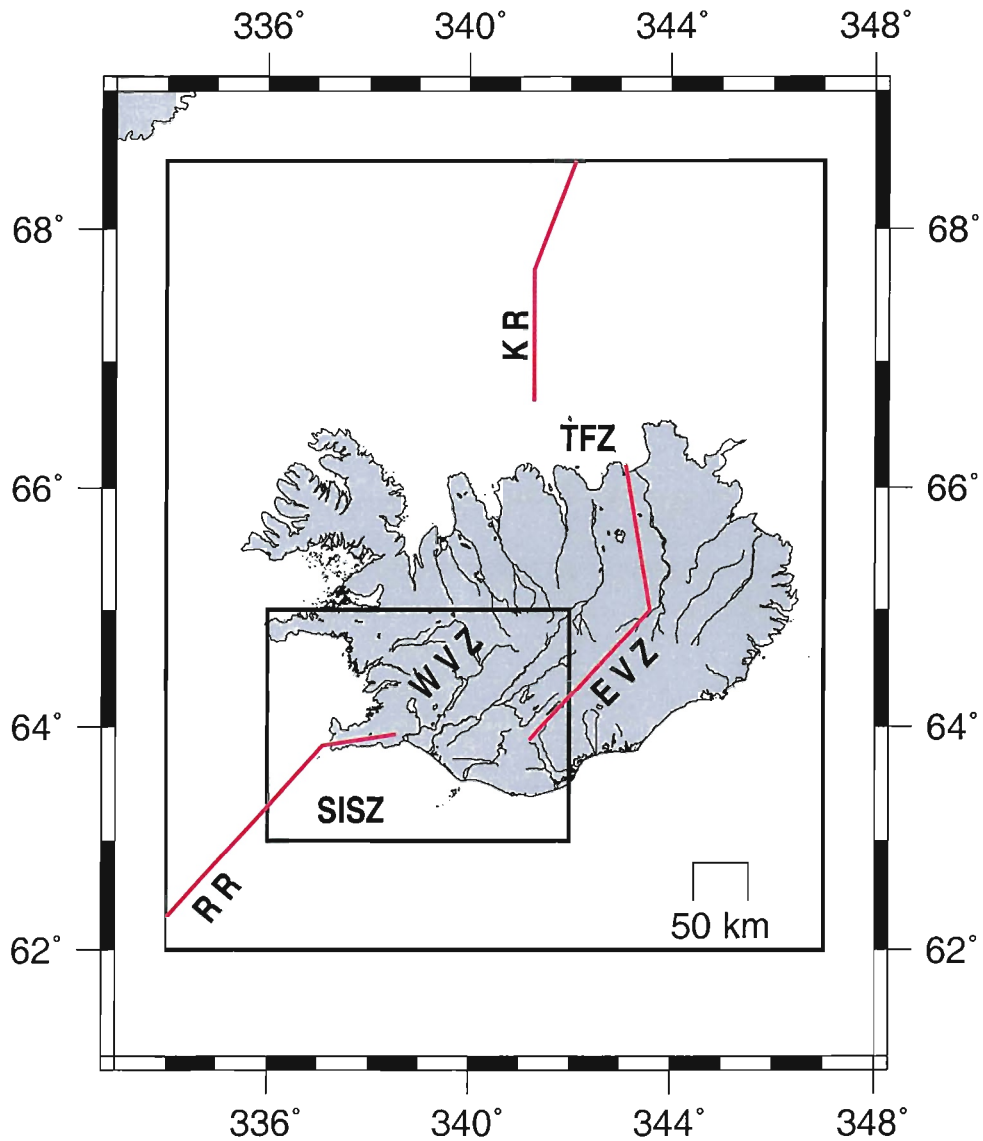


Figure 28. Map of Iceland and surrounding area. Thick red lines indicate mid-Atlantic ridge segments, as used in the PRENLAB-2 modelling. The E-W segment, continuation of RR, was not assumed in the PRENLAB-1 model (see text). The smaller box shows the region of the model on the South Iceland seismic zone. The SISZ extends approximately between (338.6°E, 63.95°N) to (341.2°E, 64°N). The large box gives the region for the Iceland rift model.

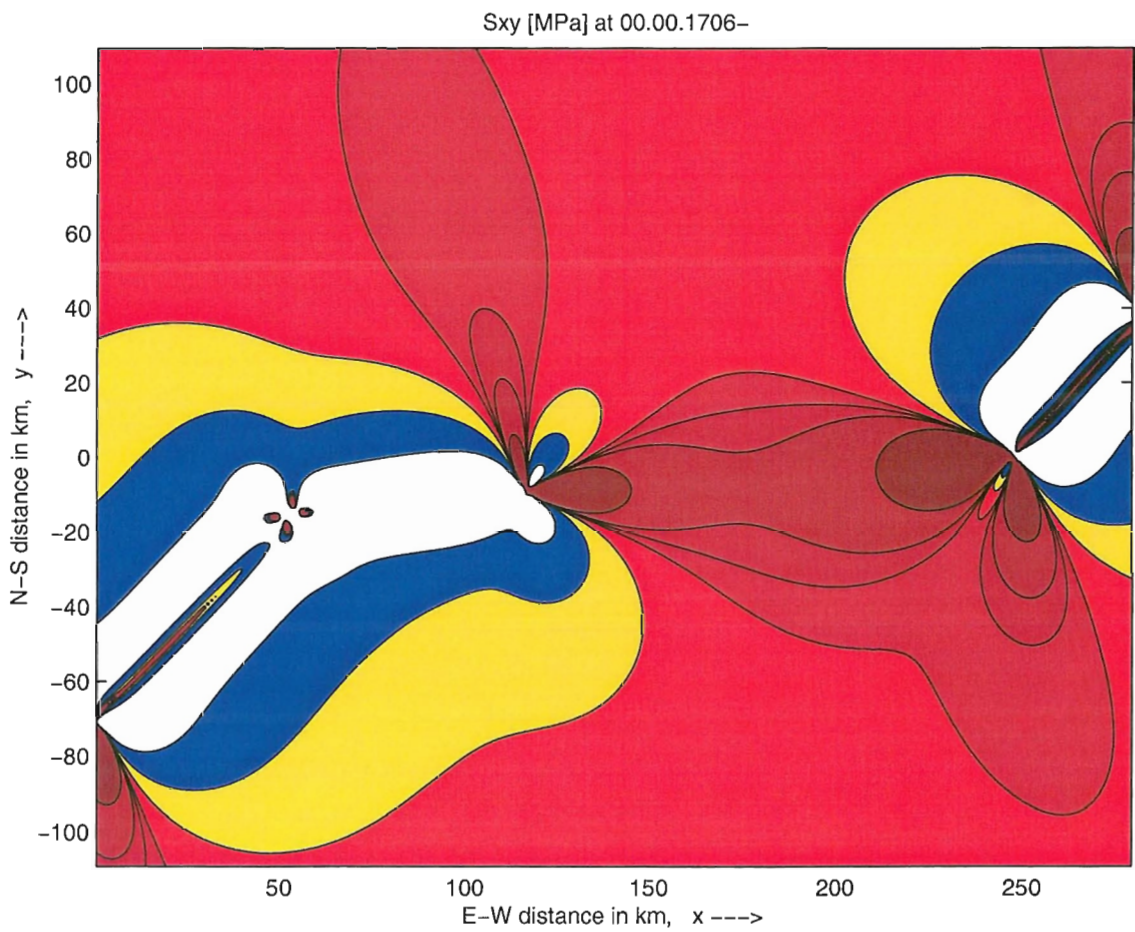


Figure 29. Shear stress field in the South Iceland seismic zone and its surroundings as assumed in 1706 ("improved model"). The isoline values are: 0, 2, 2.5, 2.7, 2.75, 2.8, and 3.0 MPa.

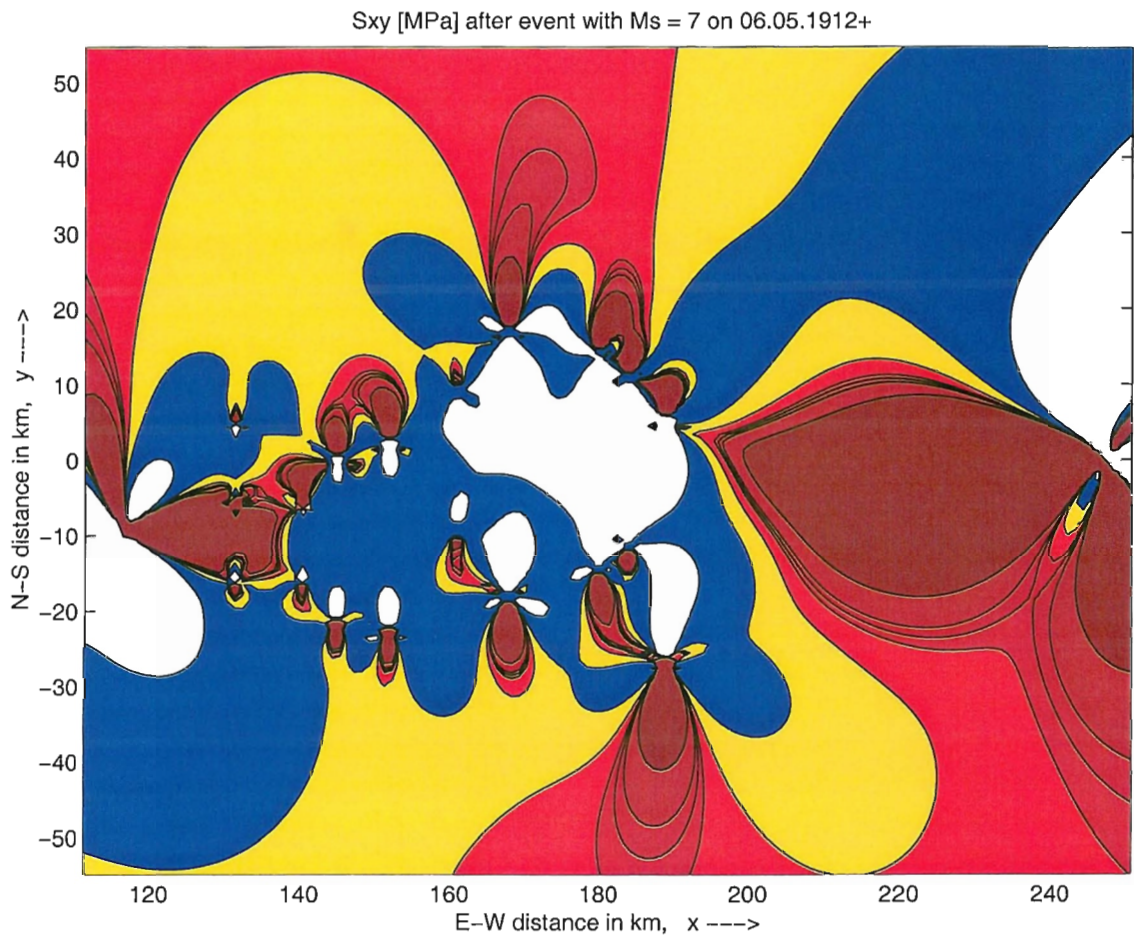


Figure 30. *The stress field after the last strong event May 6, 1912,  $M=7.0$  earthquake occurred at (187, -11) in the "improved model". Here, only the central region of the modelled area is displayed, so that the details inside the SISZ are clearly visible. The isoline values are: 0, 2, 2.5, 2.7, 2.75, 2.8, and 3.0 MPa.*

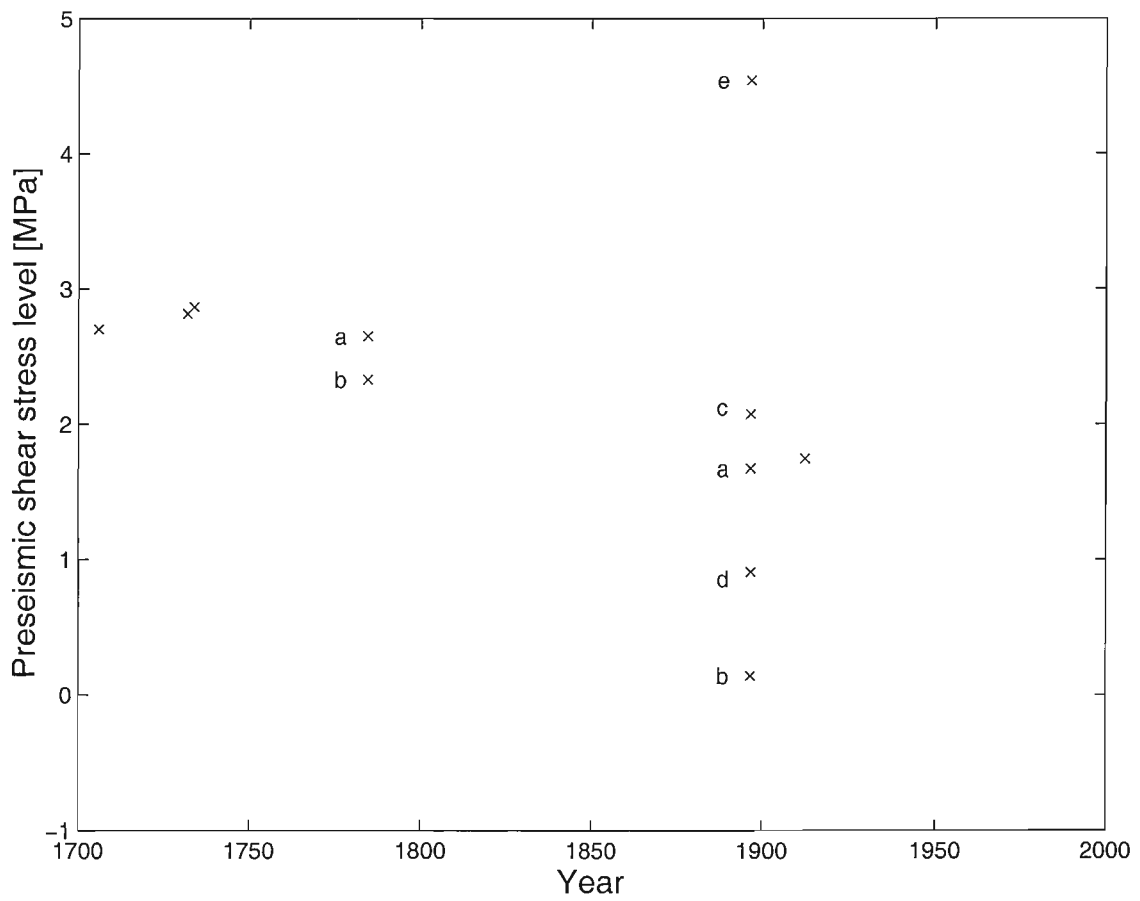


Figure 31. *Cross plot of the pre-seismic shear stress level at the site of the impending earthquakes vs. occurrence time. Here in the "improved model", the stress values at 10 to 70 test-points near the surface trace of the rupture plane were averaged. — Letters "a" through "e" denote the events in one year in temporal sequence.*

### Two problems were addressed next

1. To see how sensitive the results depend on the model parameters, it was begun to check extreme cases and their outcome.
2. The average stress level before some events is only slightly above and even below the background stress of about 2.65 MPa (see the main shocks 1706 and 1784a, and 1896a and 1912, respectively). This is, among other reasons, due to the fact that the rupture planes, used until now, extend rather far to the north and south of the SISZ.

The damage areas from historical records are not gathered by scientists and are usually biased by uneven population density. So the magnitudes and locations are not very accurate, as stated earlier. As mentioned in the footnotes of Table 5, there are doubts on the correct rupture size from global relations between magnitude and rupture length.

From both reasons, given here, a model was calculated that uses the same seismic moment of the events, but cuts the fault length to 50% while doubling the co-seismic displacement. It will be termed "short rupture model". One side-effect of this change is an increase of the stress level by a factor 2.5, as the moment release is concentrated to a smaller area. The background stress field amplitude was increased accordingly, because - as described above - this field is adjusted to the average stress change of the strongest event. It is important to note that the increase in stress level does not change the stress pattern of the initial stress field; as we are not looking for specific stress amplitudes but for stress concentrations, the change in level is not important.

The resulting pre-seismic stress level is expected to be smoother than before due to the concentration of stress release to high stress areas.

For comparison with the models above, some results obtained in the "short rupture model" are given in Figures 32 through 34.

The pre-event stress level now varies between 6.5 and 7.4 MPa for the main shocks (for more details cf. Figure 34). It is more stable than the level in the previous models, if relative values are compared. For most events, the initial stress level is considerably higher than the background. Only for two main shocks it is near the background (1706 and 1896a) and only for two strong aftershocks it is below (1896b and d). The differences to the previous model are not very large, but a further improvement of the "improved model" could be achieved in using shorter rupture planes. Concerning the extension to a layered crustal structure with an inelastic substratum to include post-seismic relaxation processes, these models will be addressed as soon as the elastic ones are finished. A new code has been prepared for this, much faster, more accurate, and capable of including even more layers than the existing code. The extension of the computer programme for the superposition of stress fields with the new code has already begun. The results will not only be compared to those from the purely elastic models, but also to continuous GPS crustal deformation data, as soon as these are available.

### **Extrapolation of the stress field calculated within PRENLAB for the next years**

The stress field for the new models was extrapolated to spring 1999, with the additional stresses due to plate motion since 1912. In the "improved model", shear stress inside the SISZ are only high at small places and at some places at the northern and southern margins of the seismically active zone. This is similar in the "short rupture model". In

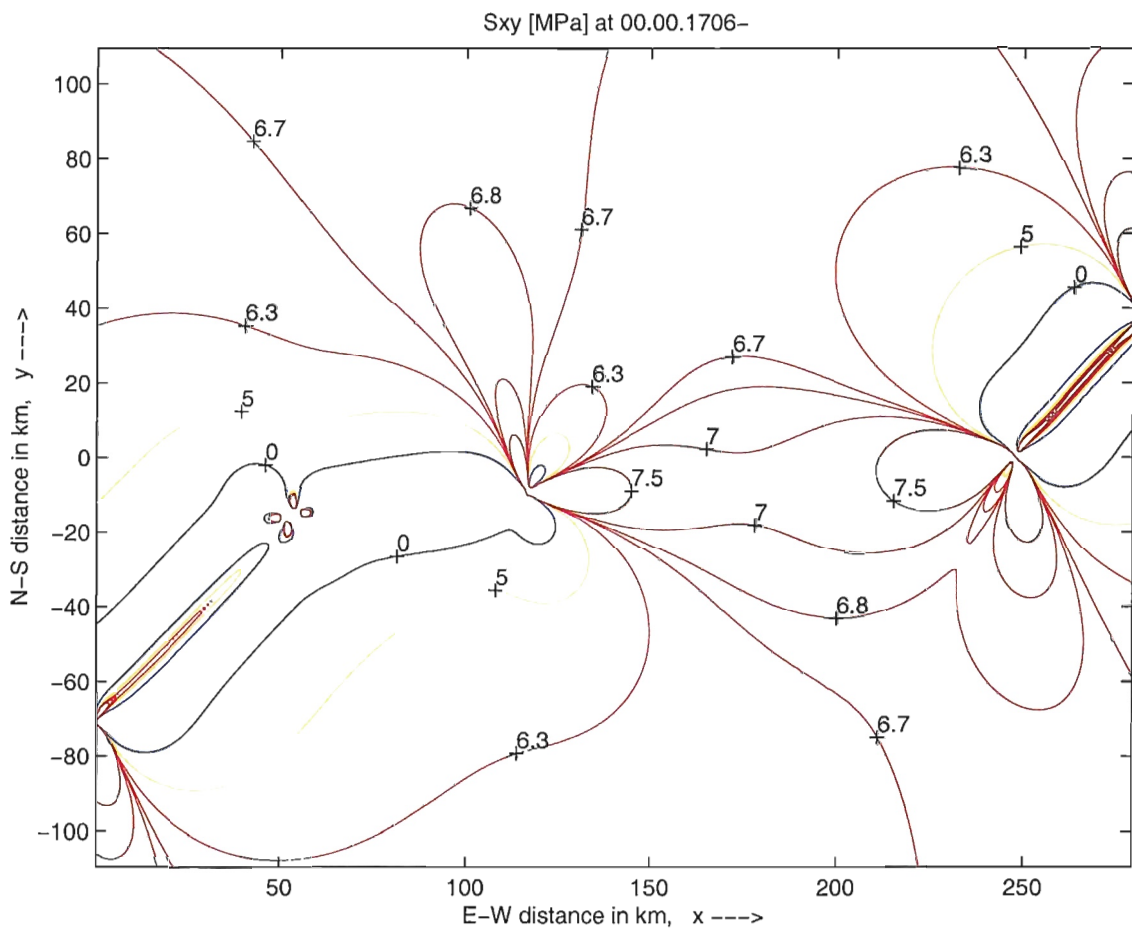


Figure 32. *Shear stress field in the South Iceland seismic zone and its surroundings as assumed in 1706 – the starting field for the model calculations in the "short rupture model". The background stress is about 6.5 MPa. It is increased between the rift tips which are at (125, -5) and (250, 0).*

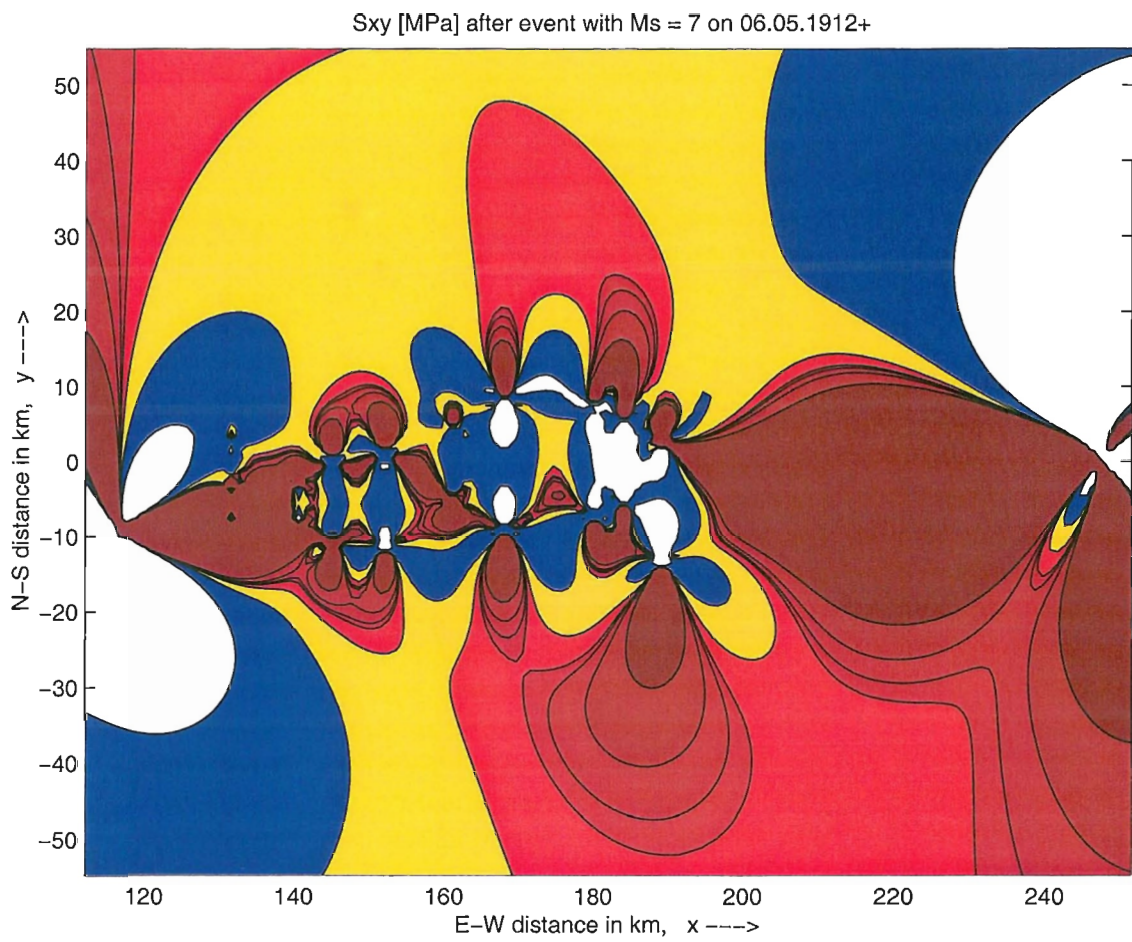


Figure 33. *The stress field after the last strong event May 6, 1912,  $M=7.0$  earthquake occurred at (187, -6) ("short rupture model"). The values of the isolines as in Figure 32 apply.*

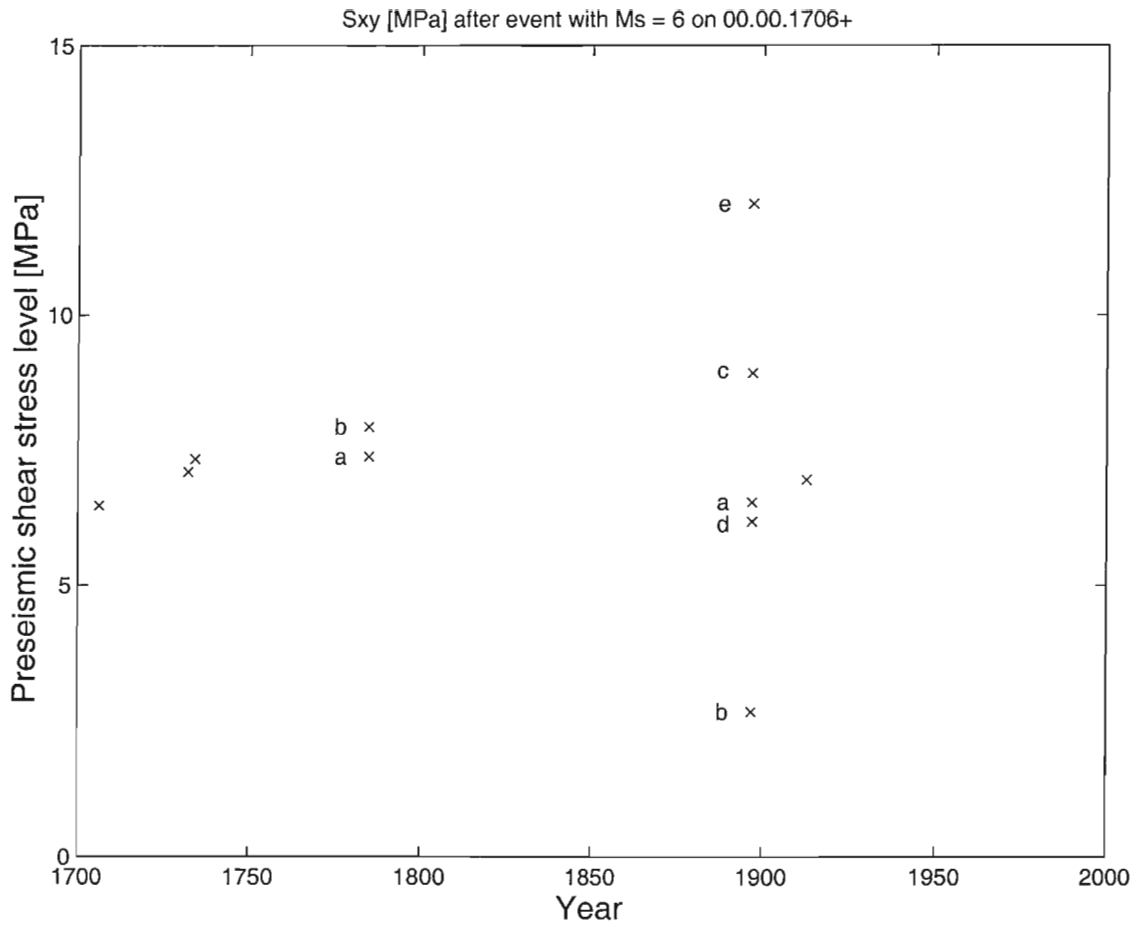


Figure 34. Cross plot of the pre-seismic shear stress level at the site of the impending earthquakes vs. occurrence time. Here in the "short rupture model", the stress values at 5 to 35 test-points near the surface trace of the rupture plane were averaged. — Letters "a" through "e" denote the events in one year in temporal sequence.

general, in the west and in the east, where the SISZ meets the ridge segments, stresses are concentrated. Is this a weakness of the models or is it the real situation?

An argument against high stress there is, that there was no large event ( $M \geq 6.5$ ) since 1706 near the ridge segments. The origin of the stress concentrations at the end of the SISZ, i.e. at the tips of the adjoining ridges, is the fact that the ridges do not extend to infinite depth, but are assumed to reach only 7 km depth and enter an inelastic, hot region not capable of supporting stresses for time periods of years. Deeper penetration of the brittle layer there would homogenize the stress field between rift tips at some average value. Entailed is the following: In the models introduced here, high initial stresses at the tips are needed to obtain high enough stresses in the center of the SISZ (see section about the initial stress field above). Further, high tensional stresses at the rifts mean high initial stress in 1706 compared to the annual increase by plate motion, as long as the rifting speed is kept constant. Indeed, if one compares the situation in 1912 with that calculated for 1999 the stress build-up by plate motion is very low. It would mean that the stress release by earthquakes in a series of events as it was observed and is modelled here, would be followed by a period of quiescence until the stress level of 1706 is reached again.

On the other hand, there are some indications that the present stress release indeed mainly takes place at the ends of the SISZ: Interestingly, in 1987, there was a strong earthquake ( $M_S=5.8$ ) at  $63.91^\circ\text{N}$ ,  $19.78^\circ\text{W}$  (198, -9) near Vatnafjöll (see Figure 27) at the east end of the SISZ. This event was not included in the modelling as its magnitude was below  $M=6$ . Nevertheless, it occurred in a region of high stress in the models. In 1998, there were 2 stronger events at the Hengill triple junction at the western end of the SISZ: June 4 ( $M=5.1$ ) and November 13 ( $M=5$ ) both accompanied by a lot of smaller events.

Considering this conflicting information, another (extreme) model will be computed during the next months using a much deeper width of the brittle layer at the rifts with the consequences of lower stresses at the ends of the SISZ and a stronger influence of the plate motion over that of the initial stress amplitudes.

### **Pin-pointing of stress concentrations in space and time**

The models yields stress concentrations for today at the western (about  $21.4^\circ\text{W}$ ,  $64^\circ\text{N}$ ) and eastern end (about  $18.8^\circ\text{E}$ ,  $64^\circ\text{N}$ ) of the SISZ and some smaller spots inside the SISZ around (150 to 160,  $\pm 10$ ) in model coordinates, i.e. around ( $20^\circ\text{W}$ ,  $64^\circ\text{N}$ ). As the stress build-up by plate motion is very low in these models, the uncertainty in time is very large in the so-called "improved model" and still large in the "short rupture model".

The high stresses at the ends of the SISZ are debatable. On one hand, there was no earthquake above  $M=6.5$  in both areas since 1706, on the other hand, the recent seismicity in both areas is high with events  $M \geq 5$  (1987 in the east at Vatnafjöll and in 1998 in the west, near Hengill).

### **Search for characteristic preseismic stress level**

As a simple assumption, one might expect, that earthquakes in a certain fault zone usually occur at about the same critical shear stress level. Here, we try to find out, if such an expectation matches the known facts about the earthquakes and the stress field in the SISZ.

In all models, the pre-seismic stress level for most main shocks is high and fairly

stable. This indicates that the rather simple model can already explain the main features of the behaviour of the SISZ. This is especially astonishing, when the fact is kept in mind, that most (all but one) events used are not instrumentally recorded. Even though the earthquake rupture planes strike N-S, the stress changes calculated here affect the whole area of the SISZ.

The tendency with time towards slightly lower values, is an indication that the stress increase due to rifting might have been assumed too low, i.e. the spreading rate between 1706 and 1912 might be higher than 2 cm/year. Moreover, the initial unknown stress field of 1706 could be reduced in the eastern part and the central part, where the first events did not occur before 1732 and 1734, respectively.

A closer look, yields that for the "improved model" the stress level before the earthquakes is between 1.9 and 2.9 MPa, if only the main shocks and no aftershocks are considered (Figure 31). However, in this model, there are 4 events with pre-seismic stress level not much above the background stress, which would not be expected. In the "short rupture model" (same seismic moment as before, but half of the rupture lengths and twice of the co-seismic displacements) the stress level is higher and the pre-event stress level varies between 6.5 and 7.4 MPa for the main shocks (cf. Figure 34). It is more stable than the level in the previous models, if relative values are compared, and for most events, the initial stress level is considerably higher than the background. Only for two main shocks it is near the background (1706 and 1896a) and only for two strong aftershocks it is below (1896b and d). So, the stress field analysis gives some indication that the strong change in rupture lengths used, means to tune the model into the right direction. Nevertheless, the strong variation in model parameters does not lead to totally different results, i.e. the model is rather stable in this respect. To further check the sensitivity of the model results to changes, a model with stronger influence of the permanent stress build-up by plate motion will be calculated next.

In general, the models go beyond the standard earthquake moment release and hazard analysis as they include the spatial location and extension of the events and provide an extrapolation to the present stress situation.

# References

- [1] Angelier, J., F. Bergerat & C. Homberg 1999. Variable coupling explains complex tectonic regimes near oceanic transform fault: Flateyjarskagi, Iceland. *Terra Nova*, submitted.
- [2] Angelier, J., F. Bergerat & S.Th. Rögnvaldsson 1999. Using inversion of large population of earthquake focal mechanisms to derive the regional seismotectonic field: Iceland. In: Abstracts from the tenth biennial EUG meeting, Strasbourg, France, March 28 - April 1, 1999.
- [3] Angelier, J., F. Bergerat & S.Th. Rögnvaldsson 1999. Perturbation of plate-scale extension across oceanic rift and transform faults revealed by inversion of earthquake focal mechanisms in Iceland. In: Abstracts from the XXIV EGS General Assembly, The Hague, The Netherlands, April 19-23, 1999.
- [4] Ágústsson, K. 1998. Jarðskjálftahrina á Hellisheiði og í Hengli í maí-júlí 1998. *Greinargerð Veðurstofu Íslands VÍ-G98040-JA06*. Report, Icelandic Meteorological Office, Reykjavík, 35 pp.
- [5] Belardinelli, M.E., M. Bonafede, & Á. Guðmundsson 2000. Secondary earthquake fractures generated by a strike slip fault in the South Iceland seismic zone. *J. Geophys. Res.*, in press.
- [6] Bergerat, F., Á. Guðmundsson, J. Angelier & S.Th. Rögnvaldsson 1998. Seismotectonics of the central part of the South Iceland seismic zone. *Tectonophysics* 298, 319-335.
- [7] Bergerat, F. & J. Angelier 1999. The South Iceland seismic zone: tectonic and seismotectonic analyses revealing the evolution from rifting to transform motion. *Journ. Geodynamics* 4(2), 1-21.
- [8] Bergerat, F. & J. Angelier 1999. Géométrie des failles et régimes de contraintes à différents stades de développement des zones transformantes océaniques: exemple de la zone sismique Sud-Islandaise et de la zone de fracture de Tjörnes (Islande). *C.R. Acad. Sc.* 329, 653-659.
- [9] Bergerat, F., J. Angelier & S. Verrier 1999. Tectonic stress regimes, rift extension and transform motion: the South Iceland seismic zone. *Geodin. Acta* 12(5), 303-319.
- [10] Bergerat, F., J. Angelier & C. Homberg 2000. Tectonic analysis of the Húsavík-Flatey fault (northern Iceland) and mechanisms of an oceanic transform zone, the Tjörnes fracture zone. *Journ. Geophys. Res.*, submitted.

- [11] Bjarnason, I.P. & P. Einarsson 1991. Source mechanism of the 1987 Vatnafjöll earthquake in South Iceland. *J. Geophys. Res.* 96, 4313-4324.
- [12] Bjarnason, I.P., P. Cowie, M.H. Anders, L. Seeber & C.H. Scholz 1993. The 1912 Iceland earthquake rupture: growth and development of a nascent transform system. *Bull. Seism. Soc. Am.* 83, 416-435.
- [13] Bonafede, M. & E. Rivalta 1999. The tensile dislocation problem in a layered elastic medium. *Geophys. J. Int.* 136, 341-356.
- [14] Bonafede, M. & E. Rivalta 1999. On tensile cracks close to and across the interface between two welded elastic half-spaces. *Geophys. J. Int.* 138, 410-434.
- [15] Bonafede, M. & A. Neri 2000. Effects induced by an earthquake on its fault plane: a boundary element study. *Geophys. J. Int.*, in press.
- [16] Böðvarsson, R., S.Th. Rögnvaldsson, R. Slunga & E. Kjartansson 1999. The SIL data acquisition system - at present and beyond year 2000. *Phys. Earth Planet. Inter.* 113, 89-101.
- [17] Crampin, S. 1998. Stress-forecasting: a viable alternative to earthquake prediction in a dynamic Earth. *Trans. R. Soc. Edin. Earth Sci.* 89, 121-133.
- [18] Crampin, S. 1999. Stress-forecasting earthquakes. *Seism. Res. Lett.* 70, 291-293.
- [19] Crampin, S. 1999. Calculable fluid-rock interactions. *J. Geol. Soc.* 156, 501-514.
- [20] Crampin, S. 1999. A successful stress-forecast: an addendum to "Stress-forecasting: a viable alternative to earthquake prediction in a dynamic Earth". *Trans. R. Soc. Edin. Earth Sci.* 89, 231.
- [21] Crampin, S. 1999. Stress-monitoring sites (SMSs) for stress-forecasting the times and magnitudes of future earthquakes. *Tectonophysics*, submitted.
- [22] Crampin, S., T. Volti & R. Stefánsson 1999. A successfully stress-forecast earthquake. *Geophys. J. Int.* 138, F1-F5.
- [23] Crampin, S., T. Volti & P. Jackson 2000. Developing a stress-monitoring site (SMS) near Húsavík for stress-forecasting the times and magnitudes of future large earthquakes, In: *Destructive earthquakes*. Proceedings of the Second EU-Japan Workshop on Seismic Risk, Reykjavík, Iceland, June 23-27, 1999, in preparation.
- [24] DeMets, C., R.G. Gordon, D.F. Argus & S. Stein 1990. Current plate motions. *Geophys. J. Int.* 101, 425-478.
- [25] Dziewonski, A.M., A.L.Hales & E.R. Lapwood 1975. Parametrically simple earth models consistent with geophysical data. *Phys. Earth Plan. Int.* 10, 12.
- [26] Einarsson, P., S. Björnsson, G. Foulger, R. Stefánsson & Þ. Skaftadóttir 1981. Seismicity pattern in the South Iceland seismic zone. In: D. Simpson & P. Richards (editors), *Earthquake prediction - an international review. Maurice Ewing Series 4*. American Geophysical Union, 141-151.
- [27] Einarsson, P. & J. Eiríksson 1982. Earthquake fractures in the districts Land and Rangárvellir in the South Iceland seismic zone. *Jökull* 32, 113-120.

- [28] Einarsson, P. & K. Sæmundsson 1987. Earthquake epicenters 1982-1985 and volcanic systems in Iceland (map accompanying the festschrift *Í hlutarins eðli*, scale 1:750000). Reykjavík, Menningarsjóður.
- [29] Einarsson, P., P. Imsland, A.K. Ingimarsson, E.R. Guðmundsdóttir, H. Hallsteins-son, H. Sigurjónsson, J. Guðbjartsson, J. Hendriks, K. Jónsdóttir, K. Ísleifsson, Ó. Hilmarsson, R.H. Sigurðardóttir, S. Hreinsdóttir & V. Roth 1998. Strike-slip faults near Geitafell in the eastern Reykjanes peninsula. In: Abstracts from the spring meeting of the Geoscience Society of Iceland, Reykjavík, Iceland, April 21, 1998. In Icelandic. Paper in preparation 1999.
- [30] Erlendsson, P. & Páll Einarsson. The Hvalhnúkur fault, a strike-slip fault mapped within the Reykjanes peninsula oblique rift, Iceland 1996. In: B. Þorkelsson (editor), *Seismology in Europe*. Papers presented at the XXV ESC General Assembly, Reykjavík, Iceland, September 9-14, 1996. Reykjavík, 498-504.
- [31] Guðmundsson, Á. 1999. Postglacial crustal doming, stresses and fracture formation with application to Norway. *Tectonophysics*, in press.
- [32] Guðmundsson, Á. 1999. Fluid overpressure and stress drop in fault zones. *Geophys. Res. Lett.* 26, 115-118.
- [33] Guðmundsson, Á., 1999. Fracture dimensions, displacements and fluid transport. *J. Struct. Geol.*, accepted.
- [34] Guðmundsson, Á. & C. Homberg 1999. Evolution of stress fields and faulting in seismic zones. *Pure Appl. Geophys.* 154, 257-280.
- [35] Guðmundsson, Á., L.B. Marinoni & J. Marti 1999. Injection and arrest of dykes: implications for volcanic hazards. *Journal of Volcanology and Geothermal Research* 88, 1-13.
- [36] Guðmundsson, Á. 2000. Dynamics of volcanic systems in Iceland: example of tec-tonism and volcanism at juxtaposed hot spot and mid-ocean ridge systems. *Ann. Rev. Earth Planet. Sci.* 28, 107-140.
- [37] Guðmundsson, Á. 2000. Fluid overpressure and flow in fault zones: field measure-ments and models. *Tectonophysics*, submitted.
- [38] Hackman, M.C., G.C.P. King & R. Bilham 1990. The mechanics of the South Iceland seismic zone. *J. Geophys. Res.* 95, 17339-17351.
- [39] Halldórsson, P., R. Stefánsson, P. Einarsson & S. Björnsson 1984. *Mat á jarðskjálfta-hættu: Dysnes, Geldinganes, Helguvík, Vatnsleysuvík, Vogastapi og Þorlákshöfn* (earthquake hazard assessment). Reykjavík, Veðurstofa Íslands, Raunvísinda-stofnun Háskólans, 34 pp.
- [40] Hreinsdóttir, S., P. Einarsson, F. Sigmundsson & Þ. Árnadóttir 1999. Measurements of continued uplift and expansion at the Hrómundartindur volcanic system. In: Abstracts from the spring meeting of the Geoscience Society of Iceland, Reykjavík, Iceland, April 20, 1999. In Icelandic.

- [41] Hreinsdóttir, S., P. Einarsson & F. Sigmundsson 1999. Crustal deformation at the oblique Reykjanes peninsula plate boundary, SW Iceland, 1993-1998, observed with GPS geodetic measurements. In: Abstracts from the AGU spring meeting, Boston, Massachusetts, May 28 - June 4, 1999.
- [42] Johnsson, D.J., F. Sigmundsson & P.T. Delaney 1999. Comment on "Volume of magma accumulation or withdrawal estimated from surface uplift or subsidence, with application to the 1960 collapse of Kilauea volcano" by P.T. Delaney and D.F. McTigue. *Bull. Volc.*, in review.
- [43] Jónsdóttir, K., P. Einarsson & V. Hjörleifsdóttir 1999. Fracture systems active in the earthquakes of 1630 and 1784. In: Abstracts from the spring meeting of the Geoscience Society of Iceland, Reykjavík, Iceland, April 20, 1999. In Icelandic.
- [44] Jouanne, F., T. Villemin & GPS-TFZ TEAM 1999. Seismic risk at the rift-transform junction in North Iceland. *Geophys. Res. Lett.* 26, 3689-3699.
- [45] Kanamori, H. & D.L. Andersson 1975. Theoretical basis of some empirical relations in seismology. *Bull. Seism. Soc. Am.* 65, 1073-1096.
- [46] Lund, B. & R. Slunga 1999. Stress tensor inversion using detailed microearthquake information and stability constraints: application to Ölfus in Southwest Iceland. *J. Geophys. Res.* 104, 14947-14964.
- [47] Meredith, P.G. 1989. Comparative fracture toughness testing of rocks. In: *Fracture toughness and fracture energy*. Balkema, Rotterdam, 265-277.
- [48] Qian, H. 1986. Recent displacements along Xianshuihe fault belt and its relation with seismic activities. *J. Seism. Res.* 9, 601-614.
- [49] Roth, F. 1989. A model for the present stress field along the Xian-shui-he fault belt, NW Sichuan, China. In: M.J. Berry (editor), *Earthquake hazard assessment and prediction*. *Tectonophysics* 167, 103-115.
- [50] Rögnvaldsson, S.Th. & R. Slunga 1993. Routine fault plane solutions for local and regional networks: a test with synthetic data. *Bull. Seism. Soc. Am.* 83, 1232-1247.
- [51] Rögnvaldsson, S.Th. & R. Slunga 1994. Single and joint fault plane solutions for microearthquakes in South Iceland. *Tectonophysics* 273, 73-86.
- [52] Rögnvaldsson, S.Th., Þ. Árnadóttir, K. Ágústsson, Þ. Skaftadóttir, G.B. Guðmundsson, G. Björnsson, K.S. Vogfjörð, R. Stefánsson, R. Böðvarsson, R. Slunga, S.S. Jakobsdóttir, B. Þorbjarnardóttir, P. Erlendsson, B.H. Bergsson, S. Ragnarsson, P. Halldórsson, B. Þorkelsson & M. Ásgeirsdóttir 1998. Skjálftahrina í Ölfusi í nóvember 1998. *Greinargerð Veðurstofu Íslands VÍ-G98046-JA09*. Report, Icelandic Meteorological Office, Reykjavík, 19 pp.
- [53] Rögnvaldsson, S.Th., Á. Guðmundsson & R. Slunga 1998. Seismotectonic analysis of the Tjörnes fracture zone, an active transform fault in North Iceland. *J. Geophys. Res.* 103, 30117-30129.
- [54] Rögnvaldsson, S.Th., G.B. Guðmundsson, K. Ágústsson, S.S. Jakobsdóttir, R. Slunga & R. Stefánsson 1998. Overview of the 1993-1996 seismicity near Hengill. *Rit Veðurstofu Íslands VÍ-R98006-JA05*. Research report, Icelandic Meteorological Office, Reykjavík, 16 pp.

- [55] Schick, R. 1968. A method for determining source parameters of small magnitude earthquakes. *Zeitschr. f. Geophys.* 36, 205-224.
- [56] Slunga, R. 1981. Earthquake source mechanism determination by use of body-wave amplitudes - an application to Swedish earthquakes. *Bull. Seism. Soc. Am.* 71, 25-35.
- [57] Slunga, R., P. Norrmann & A.-C. Glans 1984. Baltic shield seismicity, the results of a regional network. *Geophys. Res. Lett.* 11, 1247-1250.
- [58] Slunga, R., S.Th. Rögnvaldsson & R. Böðvarsson 1995. Absolute and relative location of similar events with application to microearthquakes in southern Iceland. *Geophys. J. Int.* 123, 409-419.
- [59] Stefánsson, R. & P. Halldórsson 1988. Strain release and strain build-up in the South Iceland seismic zone. *Tectonophysics* 152, 267-276.
- [60] Stefánsson, R., R. Böðvarsson, R. Slunga, P. Einarsson, S. Jakobsdóttir, H. Bungum, S. Gregersen, J. Havskov, J. Hjelme & H. Korhonen 1993. Earthquake prediction research in the South Iceland seismic zone and the SIL project. *Bull. Seism. Soc. Am.* 83, 696-716.
- [61] Stefánsson, R., S.Th. Rögnvaldsson, P. Halldórsson & G.B. Guðmundsson 1998. PRENLAB workshop on the Húsavík earthquake, July 30, 1998. *Greinargerð Veðurstofu Íslands VÍ-G98032-JA04*. Report, Icelandic Meteorological Office, Reykjavík, 5 pp.
- [62] Stefánsson, R., F. Bergerat, M. Bonafede, R. Böðvarsson, S. Crampin, P. Einarsson, K.L. Feigl, Á. Guðmundsson, F. Roth, F. Sigmundsson & R. Slunga 1998. PRENLAB - final report, March 1, 1996 - February 28, 1998. *Greinargerð Veðurstofu Íslands VÍ-G98041-JA07*. Report, Icelandic Meteorological Office, Reykjavík, 129 pp.
- [63] Tryggvason, A., S.Th. Rögnvaldsson & Ó.G. Flóvenz 1999. Three-dimensional imaging of the P- and S-wave velocity structure and earthquake locations beneath Southwest Iceland. *J. Geophys. Res.*, submitted.
- [64] Villemin, T., G. Ouillon & V. Ferber 1999. Processes of fractures pattern evolution deduced from field data: the Krafla fissure swarm and the last rifting episode in North Iceland. *J. Geophys. Res.*, submitted.